

Numerical simulation of flow and mixing behavior of solids on a moving grate combustion system

by

Sara Barone

Advisor: Prof. Nickolas J. Themelis

Submitted in partial fulfillment of requirements for M.S. Degree in Earth
Resources Engineering
Department of Earth and Environmental Engineering
Fu Foundation of Engineering and Applied Science
Columbia University

April 2015

Research supported by

COLUMBIA UNIVERSITY

EARTH ENGINEERING CENTER



Numerical simulation of flow and mixing behavior of solids on a moving grate combustion system

EXECUTIVE SUMMARY

The residence time of the waste particles on a moving grate is a very important parameter, and to a large extent influences the combustion process. Municipal solid waste (MSW) is not a uniform fuel, it varies widely in chemical composition and physical properties. Determining the particle residence time is a difficult task requiring pilot or industrial scale experimental work. Trying to minimize time and capital investment, mathematical models have been developed for the mixing process of a moving bed, estimating residence time of its particles, burnout rate, and evaporation parameters. In the past, the adjustment of the waste-to-energy power plants was accomplished empirically by studying the response of the system on changing operation parameters. However, numerical simulations have been established for the modeling of material and gas flows in the presence of chemical reactions. It is a very effective tool, since it is much less costly to perform simulations than run furnace experiments.

At the present time, it is impossible to model a complete waste-to-energy combustor with the currently available commercial programs due to the complex interaction of the solids in the moving bed and the gas phase passing through the bed or flowing above it (Nakamura M. 2008). Hence,

developing appropriate tools is necessary for the description of the combustion reactions in waste combustion plants. In this study, the waste combustion on the grate and the furnace is modeled. The motion of the grate and the force of gravity transport the waste material in the cross flow to a gaseous fluid. The average residence time of the material can be influenced by adjustment of the bed height and the local transport velocity. Furthermore, an adequate mixing is necessary to provide continuous contact between gases and solids. In order to achieve these conditions, several different grate designs are in use. Based on ESyS-Particle HPC (Discrete Element Method code), granular flow and mixing on different types of waste-to-energy grates are studied in two dimensions. Discrete element simulation provides detailed information on particle positions and velocities over time. This information is used to derive quantities characterizing the dynamic process of mixing. The mixing parameters are used to compare the mixing process on different grate designs.

On the basis of the model results, it was concluded that mixing on a roller grate is much more localized than mixing on a reverse acting grate. The time-averaged velocity dependent properties $P_i^t(x)$ were averaged over the grate length to obtain the overall mixing. This total mixing property was shown to be more intense for the roller grate than for the reverse acting grate. The more distributed mixing on the reverse acting grate is also apparent when

comparing the fluctuation of the normalized depth based property $M'(x)$. The dynamics of segregation on both grate designs show the same pattern.

Further research is necessary to collect information related to transportation of the waste material in the cross flow to a gaseous fluid modeling the furnace. An established commercial CFD/FLUENT code is suggested for use. To get a closer simulation of the combustion plant, the furnace model should be coupled to a model of the waste combustion on the three most prominent types of moving grate: The forward reciprocating grate of Von Roll, the Martin reverse-acting grate, and the roller grate (Dusseldorf System).

Table of Contents

Executive Summary	ii
List of Tables	viii
List of Figures	ix
Nomenclature	x
Chapter 1: Introduction	1
1-1. Objectives of present study.....	1
1-2. Outline of the dissertation.....	2
1-3. Overview of waste-to-energy (WTE) combustion.....	2
1-3-1. Waste combustion	4
1-3-1-1. Complete combustion.....	4
1-3-1-2. Incomplete combustion.....	5
1-3-1-3. Deficient air combustion.....	6
1-3-1-4. Excess air combustion.....	6
1-4. WTE grates.....	7
1-4-1. Introduction.....	7
1-4-2. Reverse acting grate.....	10
1-4-3. Forward acting grate.....	12

1-4-4. Roller grate.....	13
1-5. Overview of the waste-to-energy technologies.....	17
1-5-1. Unprocessed solid waste combustion technology....	17
1-5-2. Refused-derived fuel combustors	19
1-5-3. Fluidized bed combustion	20
1-5-4. Advantages/disadvantages of fluidization.....	21
1-5-5. Designs of fluidized bed boilers.....	22
1-5-5-1. Bubbling fluidized bed boilers.....	23
1-5-5-2. Circulating fluidized bed boiler.....	25
Chapter 2: Simulation techniques on previous studies.....	27
2-1. Solid waste combustion models.....	27
2-2. Combustion process models.....	31
Chapter 3: Modeling of chemically reacting flow.....	33
3-1. Introduction.....	33
3-2. Methodology.....	34
3-2-1. Mechanical motion.....	34
3-3. Heat transfer mechanisms.....	35
3-3-1. Heat conduction between particles.....	35
3-3-2. Convective heat transfer between primary air and particles.....	37
3-3-3. Radiation between particles and a wall.....	38

3-3-4. Radiation of the furnace in direction to the bed surface.....	39
3-4. Physical and chemical transformation of waste in the bed.....	39
3-4-1. Drying (moisture evaporation).....	40
3-4-2. Pyrolysis (devolatilization).....	41
3-4-3. Combustion of the volatile matters.....	42
3-4-4. Combustion of fixed carbon within the bed.....	43

Chapter 4: Discrete Element Method (DEM) numerical simulation of flow dynamics and mixing.....	44
4-1. Numerical Simulation.....	44
4-1-1. Dynamics of mixing.....	51
4-1-2. Proposal based on particles' velocity.....	51
4-1-3. Proposal based on particles' trajectory.....	55
4-2. Simulation parameters and geometric features of the roller grate.....	58
4-2-1. Conclusions for the roller grate numerical simulation.....	62
4-3. Simulation parameters and geometric features of the reverse acting grate.....	65
4-3-1. Conclusions for the reverse acting grate numerical simulation	68
4-4. Conclusions and Suggested Further Research.....	72

Bibliography.....74

List of Tables

Table 1-1: Complete combustion reaction patterns

Table 4-1: Kinetics of the Düsseldorf process

Table 4-2: Particle data

Table 4-3: Material parameters of the model for particle/particle and
particle/wall interaction

Table 4-4: Particle size distribution

Table 4-5: Kinetics of the reverse acting grate

Table 4-6: MSW flow and mixing in the reverse acting grate

List of Figures

Figure 1-1: Fate of combustion air (EPA-89/03)

Figure 1-2: Diagram of Reverse Acting Grate (Martin Grate)

Figure 1-3: Diagram of Forward Acting Grate (Von Roll type)

Figure 1-4: Diagram of Roller Grate (Duesseldorf type)

Figure 1-5: Photograph of six-drum roller grate

Figure 1-6: Complete medical waste combustion system with baghouse and
wet scrubber (Enercon, Ohio)

Figure 1-7: Bubbling fluidized bed boiler

Figure 1-8: Circulating fluidized bed boiler

Figure 2-1: The volume distribution of various defined components bed

Figure 3-1: Heat conduction between two smooth-elastic spheres

Figure 3-2: Radiation from particle i to all neighboring particles

Figure 4-1: Two dimensional sketch of roller grate

Figure 4-2: Time-averaged horizontal, vertical and total mixing parameters the
grate length

Figure 4-3: Time-averaged mixing parameter over the grate length

Figure 4-4: Average normalized depth for different particle diameters

Figure 4-5: Two dimensional sketch of reverse acting grate

Figure 4-5: Time-averaged horizontal, vertical and total mixing parameters the
grate length

Figure 4-6: Time-averaged mixing parameter over the grate length.

Figure 4-7: Average normalized depth for different particle diameters.

Nomenclature

R_f feed rate of MSW in the inlet of the mass-burn WTE chamber

S particle size of MSW components

ρ particle density of MSW components

R_r frequency of reciprocating bars

L the length of the reciprocating bars travel

H height of the reciprocating bars

θ angle of the reciprocating bars

α angle of chamber bed decline

$F_{i,contact}$ particle contact force

$F_{i,Buoyancy}$ buoyancy force of a particle

$F_{i,Fluid}$ fluid drag forces

Chapter 1: Introduction

1-1. Objectives of present study

The objective of this study is to provide mechanisms for a better understanding of the dynamics of solid flow and mixing during combustion process on different WTE grate designs (e.g., reverse acting, roller, and forward acting) for the mass burn feed system.

The following steps will be taken to achieve the objective:

1. Numerical models will be used to simulate flow and mixing processes on the roller grate and reverse acting grate.
2. A comparative analysis of the outcomes will then be accomplished.
3. The waste bed model output will be coupled to the furnace model output to study the relationship of solid waste particle flow and mixing and transport and combustion phenomena.

The study may inform, through optimal grate selection and design, how to improve overall process design and efficiency of WTE power plant. The models will be validated by comparison of the results with those from similar studies.

1-2. Outline of the dissertation

This dissertation consists of six chapters. This chapter introduces a background of the WTE combustion processes and review of WTE grate technologies. Chapter 2 describes most of the previous studies done in numerical modeling of the waste bed and WTE combustion process. Chapter 3 is a Discrete Element Method (DEM) numerical simulation applied to two different types of grate, comparing the flow and mixing of particles on these two traveling grate systems. Chapter 4 shows the modeling of chemically reacting flow for the reverse acting and the roller grate systems. Chapter 5 is the coupling of the DEM and CFD models. The final chapter concludes with major findings and limitations, including suggestions for future work. The summary of this study is shown at the beginning of this dissertation.

1-3. Overview of waste-to-energy (WTE) combustion

The basic principle of solid waste combustion is similar to that of conventional fossil fuel combustion. It is imperative to understand the combustion process entirely in order to effectively design, operate, and control combustion chambers. The key areas involved in the combustion process are:

- Mass Balance over a section of a combustion chamber or the entire reactor equates the amounts of products formed by the reaction to the reactants;
- Energy Balance over a section of a reactor or the entire reactor equates the chemical energy released by the combustion of the reactants to the energy contents of the products plus the energy transferred through the walls of the combustion system;
- Thermodynamic analysis: reveals information about the composition of reagents and products as a function of temperature at equilibrium; however, it does not reveal how rapidly these changes will occur;
- Kinetic analysis: provides information on how quickly changes can occur; it determines the residence time required for a particular reaction and for a desired mass flowrate of feed materials, the size of the grate and the dimensions of the combustion chamber;
- Heat transfer by conduction, convection, and radiation: these determine the temperature distribution within a combustion system and through the surrounding walls of the system;

1-3-1. Waste combustion

1-3-1-1. Complete combustion

Complete combustion is also known as stoichiometric combustion. It is combustion process in which all carbon and hydrogen elements in the reactants are converted into;

- carbon dioxide and water in the products and no free oxygen remains in the products of combustion (flue gas);

Waste elements	Conversion products
Hydrogen, H	H_2O
Carbon, CO	CO_2
Chloride, Cl	HCl or Cl_2
Fluoride, F	HF or F_2
Sulfur, S	SO_2
Nitrogen, N	N_2
Alkali metals	Carbonate
Sodium, Na	Na_2CO_3
Potassium, K	KOH
Non-alkali metals	Oxides
Copper, Cu	CuO
Iron, Fe	Fe_2O

Table 1-1 Complete Combustion Reaction Patterns.

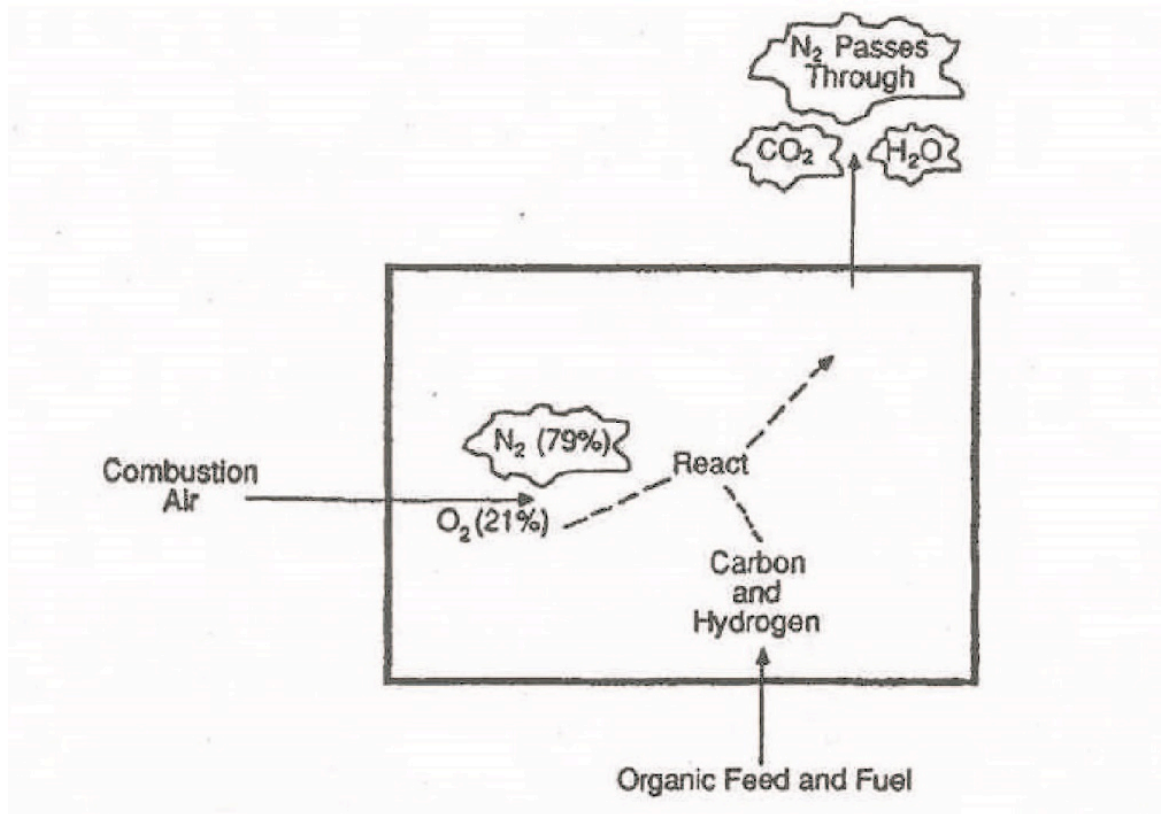


Figure 1-1: Fate of combustion air (EPA-89/03).

1-3-1-2. Incomplete combustion

Many factors can lead to incomplete combustion, such as poor mixing, a lack of combustion air, low temperatures, etc. Under these conditions, undesirable by-products may be discharged with ash or emitted with stack gas.

1-3-1-3. Deficient air combustion

When the supplied combustion air is less than that required for stoichiometric combustion. Insufficient air will result in incomplete combustion, with emissions of pollutants such as carbon monoxide, solid carbon particulates in the form of smoke or soot, and unburned and/or partially oxidized hydrocarbons. Similar emissions of pollutants also can occur in the presence of adequate air, if:

- the oxygen is not readily available for the burning process, as a result of inadequate mixing or turbulence;
- the flame is quenched too rapidly;
- the residence time is too short.

These items need to be considered carefully to have an efficient combustion process and low pollutant emission.

1-3-1-4. Excess air combustion

The amount of excess air is normally expressed as a percentage of the stoichiometric air necessary for the compound complete combustion.

Excess air is the air supplied in excess of the amount necessary for complete combustion.

$$\% A_s = (A_a/A_s)(100)$$

And:

$$\%A_e = [(A_a-A_s) / A_s](100)$$

where:

A_s = moles of stoichiometric air used at 100% of stoichiometric combustion

A_a = moles of actual air

$\%A_s$ = stoichiometric air

$\%A_e$ = excess air

1-4. WTE grates

1-4-1. Introduction

Mass burn facilities utilize hydraulically controlled reciprocating stoker grate or roller grates to move the waste through the combustion chamber. The grates typically include three or more sections which can be controlled separately. On the front end of the grate (referred to as the “drying grates”) the moisture content of the waste is driven out and the solids reach the ignition temperature. The middle section of the grate, referred to as the “burning grates”, is where the majority of active burning takes place.

The third grate section, referred to as the burnout grates, is where remaining combustibles in the waste are burned. Bottom ash is discharged from the burnout grate into a water-filled ash quench pit. From there, the wet ash is discharged by a ram or drag conveyor to a conveyor system which transports the ash to a load-out or storage area prior to disposal. Dry ash systems, which have been used in some designs, require a suitable dust collection system to prevent discharge of dust to the environment.

The stoker grates transport the refuse through the furnace and, at the same time, promote combustion by adequate agitation and good mixing with combustion air, while being cooled by the underfire air. Abrupt tumbling caused by the dropping of burning solid waste from one tier to another promotes combustion.

This action, however, also contributes to carryover of particulate matter with the existing flue gases. So, the grate is an integral part of the furnace design, acting as a hearth of the plant, where the fuel is converted into energy. The grate is the bottom of the furnace. There are many variations of grates used in WTE facilities e.g., forward acting inclined, reverse acting inclined, roller grate, and horizontal grate, but the dominant design is the Martin reverse-acting grate. Grate systems ensure that waste remains in the incinerator for the proper time and is moved around enough to expose all surfaces to the combustion heat. Combustion is initially by radiation from the active

combustion areas onto the incoming waste, resulting in drying the exposed surface and raising it to the ignition temperature. Combustion air is added from beneath the grate sections through underfire air plenums, which is also called the primary air usually one per grate section, to permit proportioning of the air supply as needed to control burning and heat release from the waste bed. The primary air is also needed to cool the grates. The grates may be divided in multiple parallel sections, each with a controllable air supply. It may be preheated to compensate for moisture in the MSW. The tendency for slagging waste components (ash and glass) causes fouling and deterioration of the furnace refractory walls.

The fusion and melting temperatures of these slags limit the operating temperatures above the grates. With simple refractory walls, flame temperatures may have to be limited to as low as 982 °C. Air-cooled or water-cooled refractory walls permit operation at higher temperatures, up to 1425 °C, with manageable slagging.

Overfire air, which is also called secondary air, is injected through rows of high-pressure nozzles located on the side walls of the chamber to complete the oxidation of the fuel-rich gases evolved from the bed and reduce the temperature of the gases below the stoichiometric flame temperature. Properly designed and operated overfired air systems are essential for good mixing and burnout of organics in the flue gas. Typically 80-100 percent

excess air is needed to control the temperature of the gases leaving the combustion chamber. The flue gases leaving the combustion chamber pass through the waterwall-cooled furnace section which cools the gases, from temperatures from 1200°C to 1425°C, generally to about 815°C before they enter the superheater and/or convection sections, to minimize the formation of slag on the tubes. The superheater and convection sections are followed by economizer sections, altogether cooling the gases to about 230-290°C before they enter the air pollution control device.

1-4-2. Reverse acting grate

The reverse acting grate moves fresh waste into the middle of the grate where it ignites and begins to burn. Once it is burning, the grate moves it back and mixes it with fresh waste, which then ignites and is moved back into the middle.

A typical reverse acting grate is 7 meters long, consists of a total of 15 bars and is inclined 26 degrees to the horizontal. The bars are positioned at an angle of 13 degrees from the traveling bed. Eight of the 15 bars are reciprocating and move a distance of 0.42 m (420 mm). The frequency of motion of the reciprocating bars can be adjusted from 10 to 50 double strokes per hour. A typical operating frequency in a WTE unit is 12 strokes per hour but the frequency used depends greatly on the composition of the MSW feed.

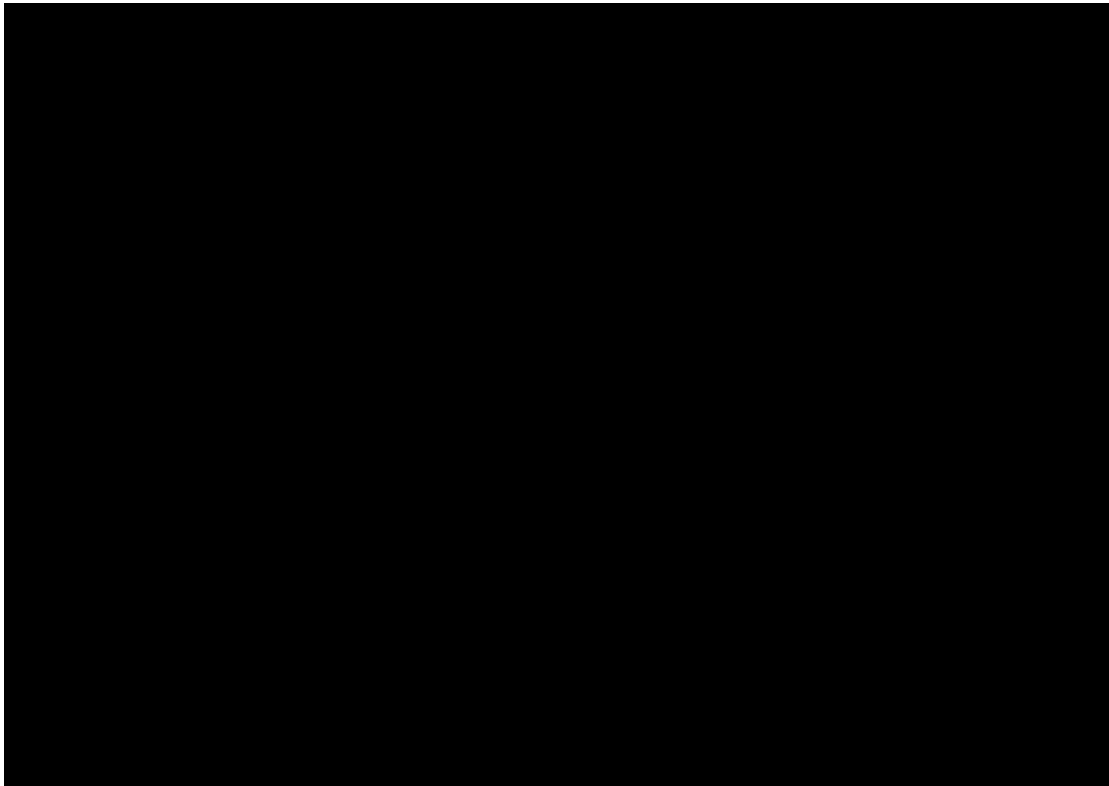


Figure1-2: Diagram of Reverse Acting Grate (Martin Grate)

A typical feed rate of MSW into the combustion chamber is 18.1 metric tons per hour (WTE of 480 short tons per day capacity). The average density of MSW is 500 lb per yd³ or 173.2 kg per m³ (Tchobanoglous *et al.* 1993) .Therefore, the corresponding volumetric feed rate of MSW is 104.8 m³ per hour. A typical ratio of the downward volumetric flow rate of MSW feed to the upwards flow of waste due to the motion of the reciprocating bars (volume of material pushed upward by the bar motion) is approximately 5/1.

1-4-3. Forward acting grate

In the forward acting grate; the stocker grate bed is composed of partially overlapping rows of bars, with alternating moving and fixed bars. As show in Figure 1-3 moving bars reciprocate the same direction with the inlet flow of waste. Waste is fed to the left-hand side of the grate and flows to the right. The moving bars oscillate, and push the waste from one bar step downstream to the next. The fixed bars are attached to a rigid support frame, while the movable bars of each section are mounted on a common frame, usually driven by a reciprocating hydraulic cylinder. The waste transport and mixing are accomplished by large spinning drums in the rotating-drum grate system. Drum rotation occurs clockwise for left-to-right waste flow. The air supply and drum speed to each section are independently controlled. Variations of these systems are sometimes employed, depending on the application involved. For example, if the waste has a material that is difficult to combust, it can be installed (Vølund) a rotary kiln immediately after the last bar section and before the ash-handing system. This procedure will provide a longer residence time needed for complete combustion. Users of this system include Combustion Engineering/DeBartolomeis, Vølund, Von Roll, and in their smaller units (≤ 170 tons per day per unit), Deutsche Babcock Anlagen (DBA). American Ref-Fuel is DBA's American licensee.



Figure 1-3: Diagram of Forward Acting Grate (Von Roll type).

1-4-4. Roller grate

The roller grate provides a sloping fuel bed, as do most European mass-burning grates for waste processing. However instead of using oscillating or reciprocating grate bars to agitate the combusting materials and to move the incombustible part down the slope, the roller grate moves the bed by slow rotation of the 1.5 m (4.92 ft) diameter drums which are formed of cast iron grate sections (Figure 1-4).

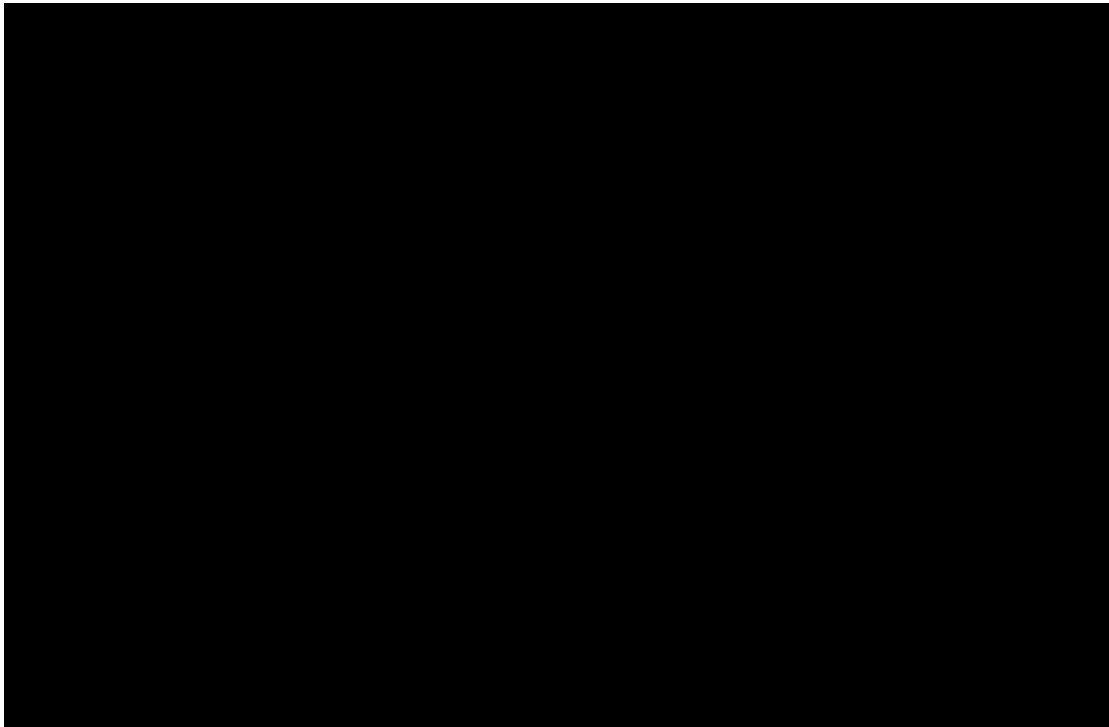


Figure 1-4: Diagram of Roller Grate (Duesseldorf type)

The drums rotate at an adjustable speed of about three to six revolutions per hour. Instead of being continuously exposed to the hot fuel bed, each grate bar rotates through a cool zone about half of the time. Thus, minimizing maintenance of the grates, the temperature of the underside of the grate is low enough to allow for repairing the drums while the unit is on line.

Each grate roll is formed of 10 sections, each of which contains 60 curved grate bars. The bars at each side which rub against the air seal plates are cast of chrome-nickel alloy to resist abrasion. Out of a total of 600 bars per roll, 20 are cast alloy.

The gap between adjacent rolls is filled by a cast iron wiper bar. This bar is strong enough to shear off waste that may become attached to the grate. Most of the grate rolls can be operated about 30,000 hours without major repairs. The wiper seals are repaired three times a year. Normal wear of the seal gradually widens the gap, which allows larger and larger pieces of residue to fall through. A screw conveyor removes such residue from underneath the grate.

Each roller constitutes a separate supply zone for primary air. The air enters the interior of the roll from both ends and flows through the many small gaps between the interlocking grate bars. The amount of air flow through each roll can be adjusted. As the combusting waste moves down the slope, the rotation speed of each successive roll is adjusted so as to keep the fuel bed thickness approximately uniform. Roller grates are strongly built. The first roll is occasionally submitted to high impact from heavy objects being fed in by the feed ram and them dropping 1.8 m (5.9 ft) to the first roll. No damage has been reported as a result of such impact. Usually it consists of six drum “walzenrost” rolls that are inclined at 30° to the horizontal.

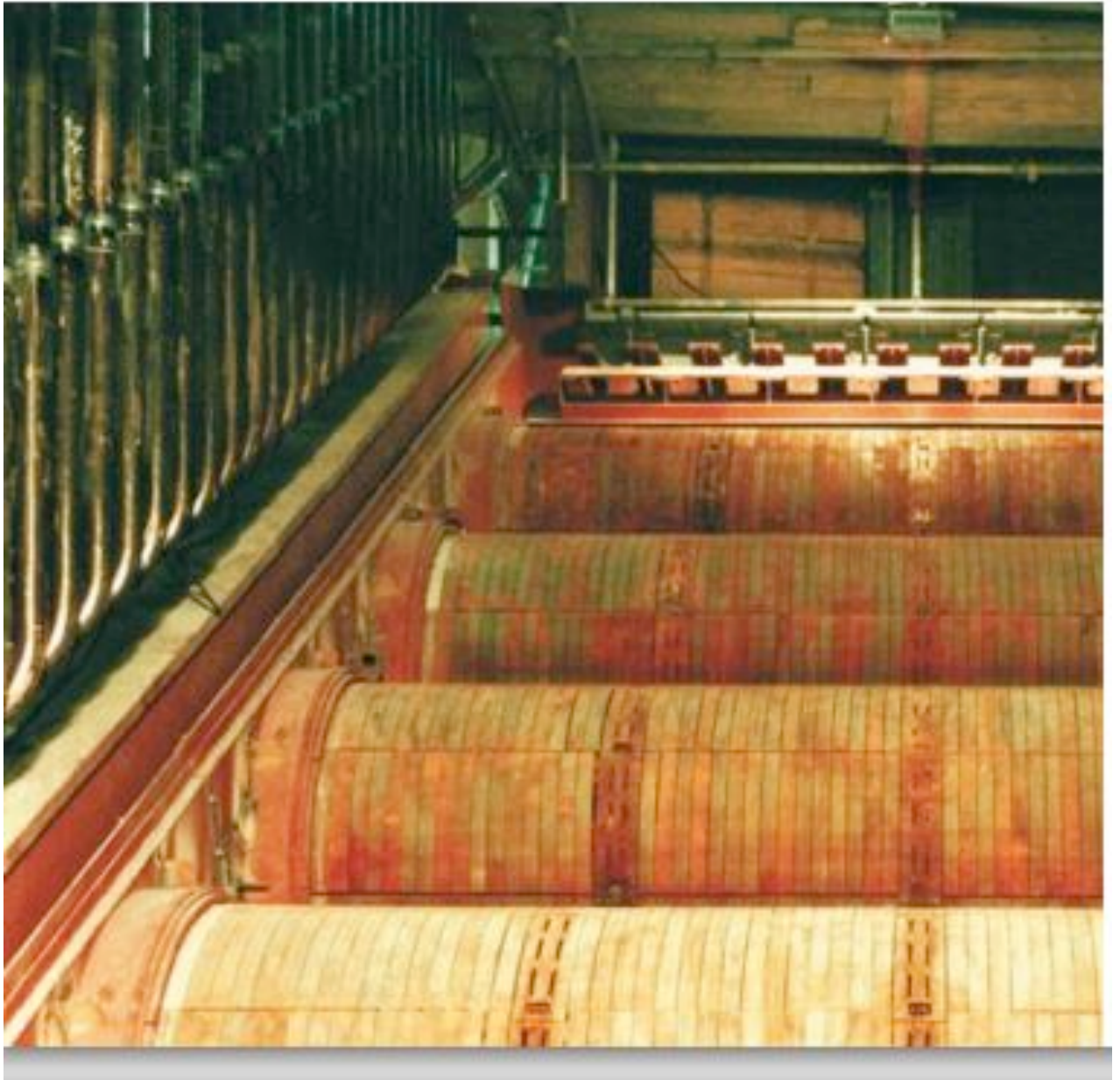


Figure 1-5: The roller grate: Six-drum roller grate), also known as the Duesseldorf grate. Cast iron wiper seals between adjacent rolls prevent large pieces of refuse from falling out of the furnace (courtesy of Vereinigte Kesselwerke.)

1-5. Overview of the waste-to-energy technologies

1-5-1. Unprocessed solid waste combustion technology (mass burn)

The Mass Burn technology includes basically three types of furnaces: water wall, water-cooled rotary combustion and controlled air furnaces. In all three types, the mass burning of MSW takes place first on a grate system that provides combustion air through the fuel bed, and with different ways of supplying fuel to the grate. The mass burning technology is most commonly applied because of its relatively low capital cost and simplicity. This technology only requires limited preparation to remove some oversized and non-combustible items. This process requires significant fuel preparation (Kumar Sudhir, 2000).

These systems range in capacity from 50-1000 tpd of MSW throughput per unit and they employ from one to three units per plant.

As seen in Figure 1-6, the waste is discharged from trucks from the tipping floor (2) to a pit (4) where the crane (5) transfer it to the feed hopper (6) from which it is injected onto the stoker grate in the primary combustion chamber (7). The ash residues pass through a quench tank (8) and into an ash hopper

(9). In some plants, these residues are passed under a magnet to separate ferrous metals. The hot gases leaving the combustion chamber pass through a waterwall furnace (10) and through a boiler, superheater and economizer (11 and 12). In the conditioning tower (13), the gases are cooled before entering the lime reactor (14). The gases then pass through the fabric filter (15) and the induced draft fan that discharges them to the stack (16).

Facilities with spray-dry scrubbers use the vessel (14) to cool the gases and evaporate the lime slurry before they enter the fabric filter. The fly ash removed from the baghouse may be either mixed with the bottom ash or disposed of separately. The fly ash is stored for use as a cement supplement, or mixed with the quench tank ash for discharge to the landfill.

The combustor walls are constructed of steel tubes that contain circulating pressurized water used to recover heat from the combustion chamber. In the lower actively burning region of the chamber, where corrosive conditions may exist, the walls are generally lined with refractory. Heat continues to be recovered in the convective sections, superheater and economizer of the boiler.

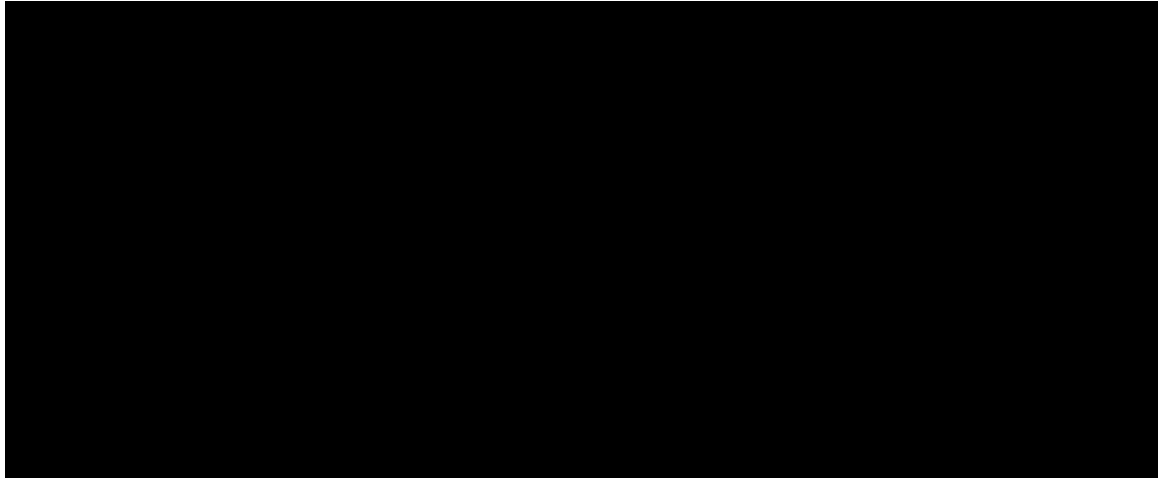


Figure 1-6: Complete medical waste combustion system with baghouse and wet scrubber (Enercon, Ohio).

1-5-2. Refused-derived fuel combustors

Refused-derived fuel combustors (RDF) burn processed waste suitable for combustion in stoker-fired boilers, similar to those used to burn granular coal in utility boilers. The waste processing system consists of a tipping floor, where front-loaders move the waste after being dumped from trucks into piles, or to the feed conveyor that leads to shredding, magnetic separation and screening operations. Systems that perform a high degree of processing to remove glass may produce as much as 20% residue, which is normally landfilled. This process increases the heating value of the remaining RDF product.

RDF fired boilers can totally avoid the use of refractory by extending the water-cooled walls down to the grate level. Corrosion-resistant alloy cladding

is used on the waterwalls to provide long life. The boilers have tall furnace chambers, providing retention time to burn out the RDF particles, followed by the superheater, convector and economizer sections, which reduce the gas temperatures to roughly 230°C. Excess air provided is typically 40-80%, similar to that of mass burn waterwall units.

1-5-3. Fluidized bed combustion

Fluidized bed technology is not new but has been revived because of fuel costs and the availability of poor quality fuels. It is used for a wide range of processes. These include fluid catalytic cracking, which is used by companies like Exxon, Texaco, and Kellogg. It is also used in chemical production, for example, in oxidizing naphthalene to obtain phthalic anhydride. Fluidization is also used to produce polyethylene. Some other uses of fluidization are coating, thermal cracking, gasification and combustion of solid waste. According to Kunii and Levenspiel, Fluidization converts a bed of solid particles into an expanded, suspended mass that has many properties of a liquid.

Fluidization occurs in stages. The first stage is known as a fixed bed, where the solid particles are mainly stationary. At higher flow rates an expanded bed can occur, where particles start to vibrate minimally and the velocity continues to increase. The bed is at minimum fluidization when, at a particular point, the velocity increases and the pressure drops.

Fluidization depends on the size of the particle and the air velocity. At low air velocities, a dense defined bed surface forms and is usually called a “bubbling fluidized bed”. Operating in higher velocities, the bed particles leave the combustion chamber with the flue gases so that solids recirculation is needed for keeping the bed solid. This type of fluidization is called “circulating fluidized bed”. The average solids velocity increases at a slower rate than does the gas velocity. With a larger increase in gas velocity, the average slip velocity decreases once again. Fluidized Bed Combustion combines high efficiency combustion of low-grade fuels with reduced emissions of sulfur and nitrogen oxides (SO_x and NO_x). The units can be designed to burn a number of fuels including low grade coals, lignite, coal mine wastes (Culm), refinery gas, woodwastes, waste solvents, sludge, etc. Fluidized bed combustion technology allows the combustion of high sulfur coal and meets environmental requirements without the use of scrubbers.

1-5-4. Advantages/disadvantages of fluidization

Fluidization works well for large scale operations, it has higher mass transfer and heat rates compared to other alternatives, and it is resistant to temperature change (Turns, S. R, 2000). The heat capacity is large, which stabilizes and maintains combustion and allows very fuel flexible operation, especially the tolerance for fuel moisture variation. It is easy to add or subtract large quantities of heat in the fluidization process because solids are

circulating in it, and the surface areas required in the heat exchangers are small.

Fluidized bed is simple and easy to operate. There are no moving parts and usually the level of automation for the boiler enables even unmanned operation. Availability is very high and usually non-scheduled outages are required in addition to an annual 10-days service stop.

The disadvantages of using fluidization are damage to the equipment from abrasion of the particles. Another problem is when large bubbles form in the reactors due to excessive gas flow, and create violent surges in the bed (Slugging).

This phenomenon decreases the efficiency of the system, because wastes energy and reactants used ("Using Chaos", 1996).

1-5-5. Designs of fluidized bed boilers

There is no unique configuration for fluidized bed boilers they could have designs depending on bed pressure, gas velocity, if the boiler has natural or assisted circulation and fuel and air distribution systems.

1-5-5-1. Bubbling fluidized bed boilers

A deep fluidized bed boiler is a bubbling bed design; the bed depth is about three to five feet deep, the average the pressure drops is approximately one

inch of water per inch of bed depth. The bulk of the bed consists of sand, ash, limestone, or other material and a small amount of fuel. The air is blown through the bed and its rate determines the quantity of fuel that can be reacted. The amount of air which can be blown through before the bed material and fuel are entrained and blown out of the furnace is limited. To stop fluidization the air flow needs to be reduced to the minimum fluidization velocity. The fuel feed systems are located either under the bed or over the bed. The under-bed feed requires coal usually with less than 8% surface moisture and crushed about 6mm top size to minimize plugging the pipes, the advantage of it is that with use of recycle combustion efficiency can be close to 99% ("Using Chaos", 1996). The over-bed feed system has a potential problem of using carbon in an effective way. Carbon elutriation can be as high as 10%. Some bubbling bed units have sectionalized design for load response. Some are divided with water cooled or refractory walls. When continuous control of loading is required for extended periods, the fluidized bed boiler may use more fuel to keep the bed temperature. A typical BFB boiler is a single drum steam boiler consisting of a membrane-wallet furnace and a second pass and a plate-wallet third pass. In the fluidized bed area the walls are covered with thin refractory lining to avoid erosion. The fuel is fed above the fluidized bed through air-cooled fuel feeding chutes. Combustion air is introduced as primary air for fluidization and into the furnace as secondary-tertiary air. Furnace walls as well as the fluidizing grid are of

membrane construction and part of the evaporation circuit. The superheater in this case is divided into three stages. Primary superheater is a horizontal convective tube superheater in the second pass. The secondary and tertiary superheaters are located in the upper part of the furnace. Between the superheater stages there are two steam temperatures using feed water spraying. Economizers and air preheaters are located in the third pass. The heat transfer surfaces are equipped with effective steam soot blowing. The boiler is started up with start-up burners directed towards the fluidized bed. The bed temperature at operating conditions is 800-900 C. The combustion air is supplied at 3-5 psig.

There is fluidizing grid in the furnace floor; it allows effective removal of the coarse material from the bed. This is done by discharging some bad material from the bed. In some cases this bed material is sieved and the fines returned to the boiler.

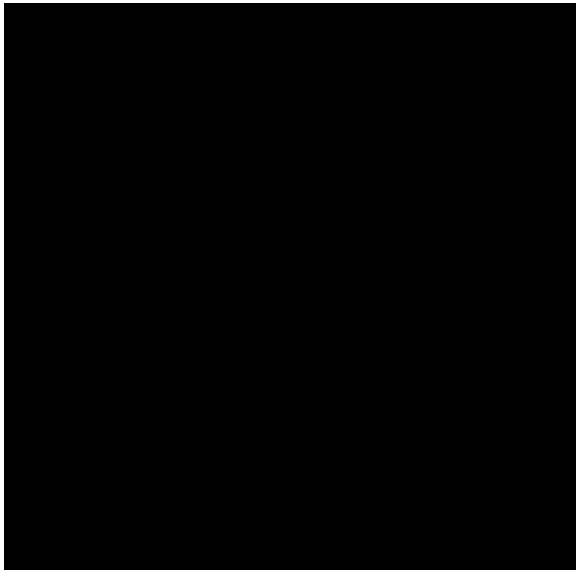


Figure 1-7: Bubbling fluidized bed boiler.

1-5-5-2. Circulating fluidized bed boiler

In a circulating fluidized bed, there is a lower combustion chamber where fuel is introduced and the first air is fed under the bed. The fuel mixed with the bed material very fast and uniformly because of the high velocity through the system. The density of the bed varies throughout the system, since when the system is operating there is not a definite bed depth. At the level where the fuel is introduced the density gets higher. To make sure solids will circulate at several levels secondary air is inserted. This process stages combustion for NO_x reduction, supplying more air to give continuity to the combustion in the upper part of the CCB. For maximum sulfur absorption combustion happens at approximately 870 ° Celsius, at a lower combustion temperature a

minimum NO_x formation takes place. The use of limestone or dolomite permits higher sulfur absorption. In a cyclone collector the dust particles are separated from the hot gases. The particles that were collected return to the combustion chamber, and ashes are removed at the bottom. The hot gases from the cyclone are discharged into the convection section of the boiler where the most of heat is absorbed to generate steam. The combustion air is supplied at 1.5 to 2 psig (Figure 1-8).

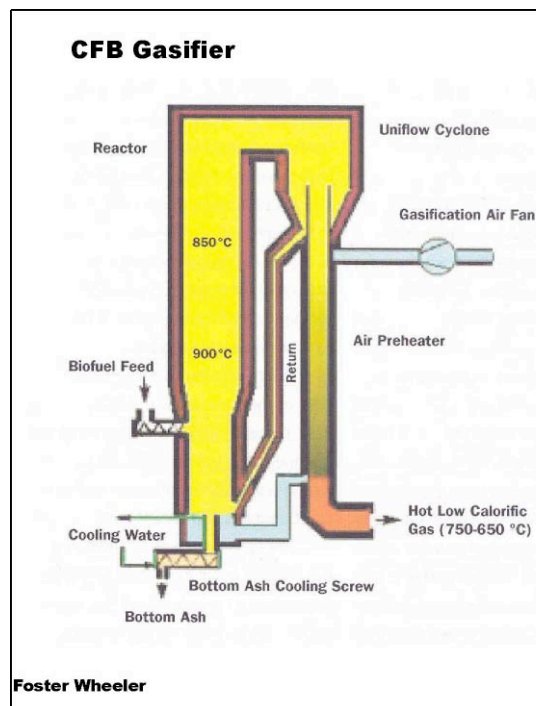


Figure 1-8: Circulating fluidized bed boiler.

Chapter 2: Simulation Techniques on previous studies

2-1. Solid waste combustion models

In previous studies there were very few methods to simulate the mixing process. Ahmed et al. (1989) developed a model taking into consideration pyrolysis reactions of the waste bed of cellulosic matter. In this study, the volume reduction process in the waste bed was considered to be proportional to the decomposition rate of the cellulose. It was assumed that the waste bed is well-mixed in the vertical direction. The heat source for the bed is the flame zone above it, and has a constant temperature. This numerical simulation calculates the pyrolysis kinetics, enthalpy of pyrolysis reactions, heat transfer by convection and radiation, kinetics and thermodynamics of volatile matter combustion, and material transport by the traveling grate. In order to examine the effects of the solid feed rates, several parameters are considered such as the air flow rates, the bed and gas temperature profiles, and the height and length of the combustion chamber required for waste conversion. The outcome of this study was an overall analysis of these processes. Beckmann et al. (1995) considered a reciprocating grate system as a serial cascade of several continuous stirred reactors. In this numerical study, the authors assumed that one of the stirred reactor elements moves along the length of the grate stoker. The grate movements are responsible for the solid matter exchange between the adjacent materials, described as

integral expressions of temperature and oxygen concentration. The conclusion of this study was that the model was successful for describing non steady combustion processes of the waste bed, and later it was used to explain the grate gasification process. Wirtz et al. (1999) proposed two approaches to model the transport and conversion of the waste during its movement along the grate. The first was a Lagrangian granular flow model that calculates the movement of individual particles, assuming continuous contact with neighbor particles. This study was not further investigated because it requires detailed information regarding fuel composition and mechanical properties of the fuel. The second approach was a Eulerian method, which transforms the movement of waste along the grate into a one-dimensional process. They assumed that the division of the waste bed in two layers and they empirically described the mass transfer between these layers along the grate. This approach was considered too simplistic a simulation of the actual grate processes.

Shin et al. (2000) also developed a one-dimensional waste bed model. On this study they consider a waste shrinkage and a two-flux radiation sub-models. The temperature on the surface of a waste bed increases in consequence of the heat transfer by radiation from the flame and furnace walls. This transport phenomenon was described in detail and compared with experimental results. The three stages of material conversion (raw waste,

reacting zone, and ash in the bed) were captured. Then, the results were implemented using a CFD simulation by Ryu et al. (Ryu et al. 2001).

Y.B. Yang and a working group from Sheffield University, UK (Yang et al. 1999, 2002) developed a waste bed model called FLIC shown in Figure 2-1. FLIC is a two-dimensional waste bed model, it was implemented with various sub-models and governing equations for mass, momentum, and heat transfer for both gases and solids. It includes Gaussian distribution of activation energies for waste devolatilization, mixing effect between volatile matter and oxidant in the volatile combustion rates, and the momentum equation for the gaseous phase. Validation of this bed model was experimentally accomplished using a bench-top batch furnace.

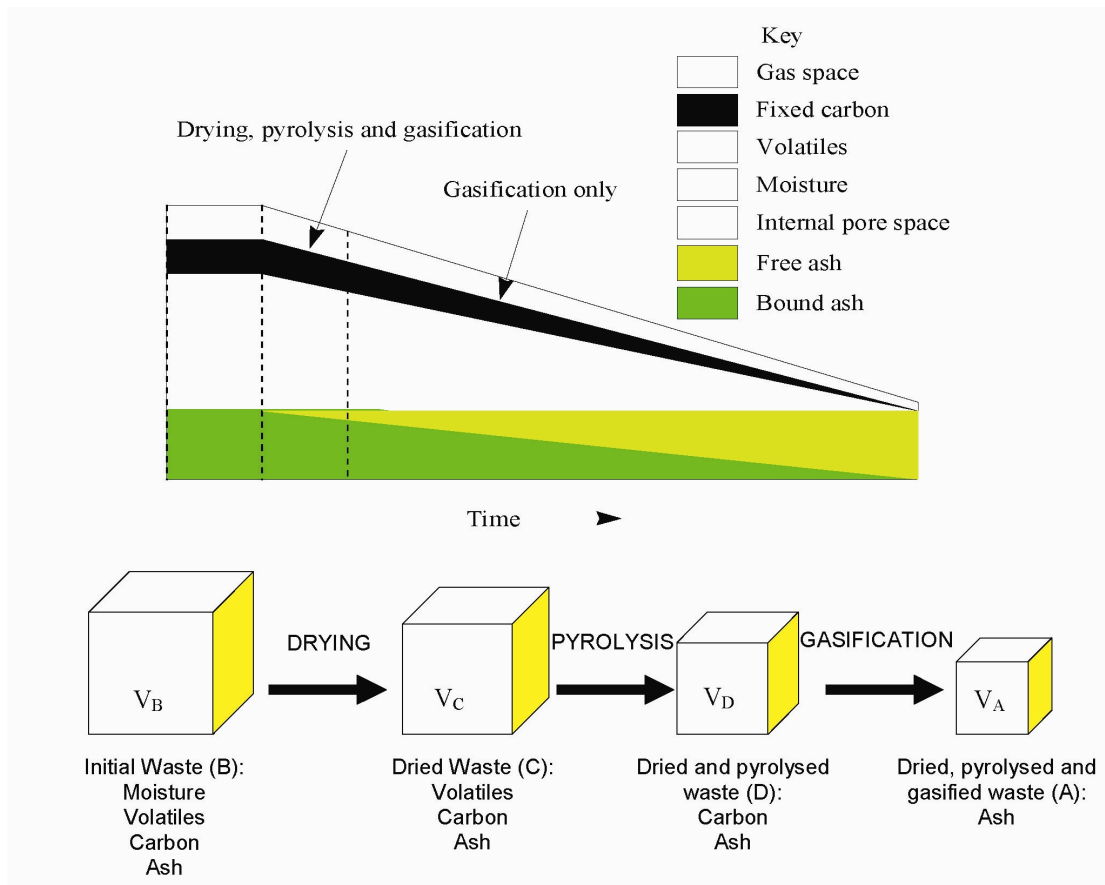


Figure 2-1 : The volume distribution of the various defined components in the bed (Yang et al. 2002).

Peters et al. (Peters 1994, Peters et al. 2005) introduced a numerical simulation to calculate three-dimensional flow and combustion process in a waste packed bed. This waste bed model simulated a bed comprised of spherical particles that mechanically interacted with adjacent particles. Using the outcome of this study, they developed a new model for mixing particles on a forward acting grate using the Discrete Element Method (DEM). This model did not include combustion processes.

Lim, C.N. (2000) developed a model using the random walk theory, for quantitative assessment of solid mixing, it describes the movement of a particle such that, at each step, the particle either stays at the origin position or moves one step to the left or to the right, ruled by a probability function.

Nakamura, M. (2008) developed a model using the Markov process for a reverse acting grate; it is a more general approach, which employs the concept of a Markov chain.

The numerical models mentioned above were accomplished for the case of a forward acting grate. Only Nakamura's work was developed for the reverse acting grate.

2-2. Combustion process models

Combustion numerical simulations using input data processed by a waste bed model have been used to analyze chemical reaction processes above the bed. Volatile matter combustion generated during the thermal conversion process of waste bed is dependent on the flow and mixing of gases and air. The chemical reactions are carried out between volatile matter and secondary air injected by arrays of nozzles on the furnaces walls. The flow of gas and air in the furnace is responsible for turbulence and mixing, and it depends on temperature, velocity, and secondary air distribution. Computational Fluid

Dynamics (CFD) is used to simulate these processes in the boiler. CFD gives solutions to fluid flows; it uses the continuity equation (conservation of mass), the Navier-Stokes equation (conservation of momentum), and the energy conservation equations. It calculates air and gas flows as well as for the chemical reactions of volatiles (C_xH_y) in the furnace. Commercial CFD software such as CFX (ANSYS, Inc.) and Fluent (Fluent Inc.) usually need an additional sub-program to account for waste bed combustion.

Chapter 3: Modeling of chemically reacting flows

3-1. Introduction

The heat and mass transfer and associated chemical reactions in the solid fuel such as biomass and municipal solid waste are connected to the particle motion. As the particles present on a grate firing system undergo a constant transformation due to drying, pyrolysis and char combustion, the essential heat transfer mechanisms to be considered are conduction, convection and radiation. To be able to have a more accurate MSW incinerator simulation it is necessary to have the particle transformations accounted for. As already mentioned, it is not possible to model combustion in combustion plants with commercial programs. For this reason the waste combustion on the grate and the boiler are modeled separately. For modeling the boiler, a commercial CFD of Fluent will be used. To be able to obtain a closed simulation of a combustion plant this boiler model will be coupled to a model of the waste combustion on the grate. The model used for this purpose is the open source DEM code, based on the description of discrete particles moving along the waste grate.

The DEM model generates data about the mass flow, the mass fraction of volatile matters and the temperatures of the waste bed and the gas. This information will be used as a boundary condition in the CFD boiler model. In

turn, the CFD model will provide radiation data from the gas to the waste bed. This data will be used as a boundary condition in the DEM model. The connection between the two models will be accomplished by external data files containing the data from each model.

3-2. Methodology

3-2-1. Mechanical motion

The mechanical motion was modeled in chapter 4 using equations (4-1) to (4-11). The Newtonian laws of movement are used to describe the mechanical movement of the particles. Only the force acting on the particles is necessary to solve these equations. The forces are calculated through the Soft-Sphere-Model, which assumes an overlapping of the particles during the collision. The force in the normal direction is obtained based on this overlapping. The force in tangential direction is calculated using the Coulomb friction law. According to this law, the friction force is proportional to the force in normal direction. After all forces acting on each particle are calculated, the particle's motion is determined by integrating the equations of motion numerically.

3-3. Heat transfer mechanisms

Because of temperature differences between particles, gas and wall surfaces in a granular material passed by a fluid flow, heat transfer (by the processes of conduction, radiation and convection) will occur.

3-3-1. Heat conduction between particles

The DEM model uses a methodology that was developed by Vargas et al. (2002). Assuming heat transfer by conduction, if two particles i and j are in contact, the heat transfer between those particles are expressed by

$$Q_c = H_c \Delta T_{ij} \quad (\text{Eq. 3-1})$$

where $\Delta T_{ij} = T_i - T_j$ is the temperature difference between the mid-planes of the spheres, and H_c is the contact conductivity.

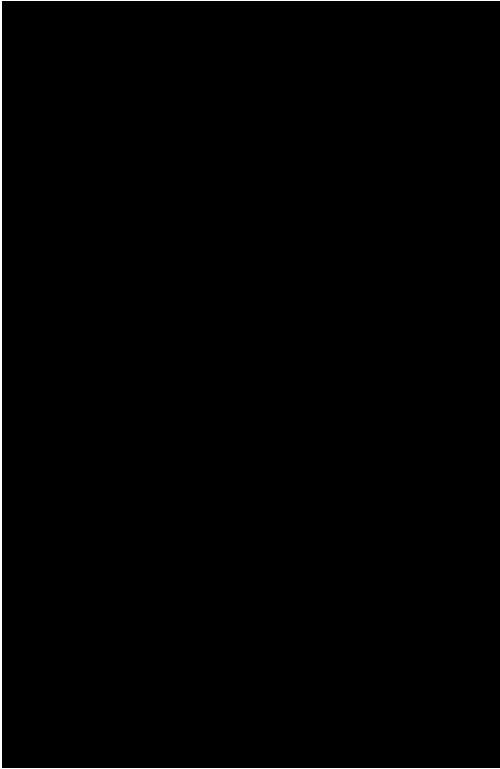


Figure 3-1: Heat conduction between two smooth-elastic spheres.

The contact conductivity for smooth-elastic sphere depends on the contact radius a obtained from Hertz contact theory, expressing conductivity by

$$\frac{H_c}{k_s} = 2 \left[\frac{3F_n r^*}{4E^*} \right]^{1/3} = 2a \quad (\text{Eq. 3-2})$$

where H_c describes the contact conductivity, F_n represents the normal force between the two contacting particles, E^* is the effective Young's modulus for the two particles, k_s the heat conductivity of the particles and r^* is the geometric average of the particle radii r_i and r_j . Particle i temperature is given by

$$\frac{dT_i}{dt} = \frac{Q_i}{\rho_i c_i V_i} \quad (\text{Eq. 3-3})$$

where T_i is the temperature of particle i , Q_i is the total amount of heat transported to particle i from particle j , and $\rho_i c_i V_i$ is particle's thermal capacity.

3-3-2. Convective heat transfer between primary air and particles

Heat transfer by convection between the primary air and particles is expressed as:

$$\dot{Q}_{conv} = \alpha_m A (T_g - T_s) \quad (\text{Eq. 3-4})$$

where α_m is the time and space averaged convective heat transfer coefficient.

T_s is the surface temperature of a particle and T_g is the temperature of the primary air. A represents the effective surface area.

3-3-3. Radiation between particles and a wall



Figure 3-2: Radiation from particle i to all neighboring particles j .

A particle i in the bulk emits radiation, which is absorbed from all neighboring particles j . The total radioactive flux a particle i emits is expressed as:

$$\dot{Q}_{rad,p-p} = \sum_j F_{i \rightarrow j} \alpha \dot{Q}_{rad,j} - \epsilon \sigma (T_s^4) \quad (\text{Eq. 3-5})$$

where α and ϵ are absorption and the emission coefficient, respectively. T_s is the surface temperature of a particle i that absorbs a radiation flux \dot{Q}_{rad} from all neighboring particles j and a wall j with the view factor $F_{i \rightarrow j}$.

3-3-4. Radiation of the furnace in direction to the bed surface

Thermal radiation from the furnace it is responsible for the initiation of the thermo chemical processes such as drying, pyrolysis and char combustion.

The specific radiation heat flux \dot{q}_{rad} that affects the waste layer is calculated using CFD/Fluent from the simulation of the furnace. This heat flux is used as a boundary condition in the DEM model. Then we will have the radiation of the furnace on a particle i of the upper waste layer specified as:

$$\dot{Q} = \alpha_i \frac{A_i}{A_t} A_i \dot{q}_{rad} \quad (\text{Eq. 3-6})$$

where A_i is the half of the sphere's surface area of particle i and A_t is the sum of all half sphere's surface areas of all accounted particles.

3-3. Physical and chemical transformation of MSW in the bed

The MSW changes in the WTE combustor are composed of three processes: drying of the surface of solid waste particles, devolatilization (where the particles soften and undergo internal transformation, releasing volatiles), and combustion of char. In the waste layer, cold particles are first heated to the water boiling point, and the temperature will then remain unchanged until the

water content is completely evaporated (drying). As the temperature starts to rise again, the volatiles are set free as combustible gases (pyrolysis). The density of the particles is continuously reduced as this process occurs. After all volatile components are released, the remaining char surface starts burning (char combustion), and its size is reduced proportionally to the mass loss until only inert ash remains. In addition to these three processes, the volatiles released from heated solid particles react with oxygen, which is called volatile combustion.

3-3-1. Drying (moisture evaporation)

The moisture content indicates the amount of water in the fuel, expressed as a percentage of the weight. For MSW, moisture content is the most critical factor determining the amount of heat that can be obtained through combustion. When burning the fuel, water needs to be evaporated first before heat becomes available. Therefore, the higher the moisture content, the lower the energy content. Drying is an endothermic process. This process is fast, but it depends on the temperature of the surrounding gas and size of the particle. The drying is assumed to be finished when the temperature of the particle is around 150°C (Hornbeck RW, 1975), it occurs at the surface of solid waste particles just after MSW is fed into the combustor. Heat is transferred by convection of the gases surrounding the waste particles and of

the primary air injected from the traveling grate into the MSW bed. The rate of solid waste evaporation can be expressed as:

$$R_{drying} = A_s h_s (C_{H_2O,s} - C_{H_2O,g}) , \text{ when } T_s < 100C^{\circ} \quad (\text{Eq. 3-7})$$

$$R_{drying} = Q_{ccr} / H_{evp} , \text{ when } T_s > 100C^{\circ} \quad (\text{Eq. 3-8})$$

$$Q_{ccr} = A_s (h_s (T_g - T_s) + \epsilon_s \sigma (T_{env}^4 - T_s^4)) \quad (\text{Eq. 3-9})$$

The Nusselt number for heat transfer and Sherwood number for mass transfer between the solid and gas phases are calculated as $Nu = 2 + 1.1Pr^{1/3} Re^{0.6}$ and $Sh = 2 + 1.1Sc^{1/3} Re^{0.6}$, respectively (Wakao and Kaguei 1982).

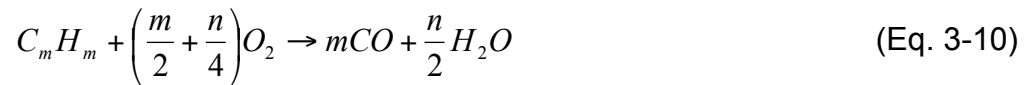
3-3-2. Pyrolysis (devolatilization)

The term pyrolysis (from *Greek* – chemical decomposition due to heating) is a decomposition process caused by the supply of energy under oxygen deficient conditions and mainly leads to the separation of volatile gases. During the devolatilization the structure of the fuel changes. Soot particles and gases (called volatiles) are released in a weakly endothermic process. After the water evaporates from the fuel and temperature rises, the devolatilization process begins. After the pyrolysis, the remaining solids are

char and ash. The composition of volatiles and the amount of char after pyrolysis depend on the heating rate. A high heating rate leads to a larger fraction of gas than a low heating rate.

3-3-3. Combustion of volatile matters

During the devolatilization process, a wide range of volatile substances is generated. This is a complex process, and it is difficult to predict the makeup and proportion of all the substances. To simplify the modeling, we may assume a representative hydrocarbon to be the only combustible product from the devolatilization process, as follows.

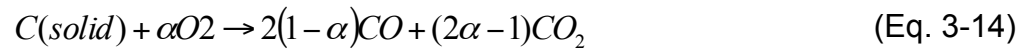


$$R_{CO} = 1.3 \times 10^{11} C_{CO} C_{H_2O}^{0.5} C_{O_2}^{0.5} \quad (\text{Eq. 3-12})$$

$$R_{C_m H_n} = 59.8 T_g P^{0.3} C_{H_2O}^{0.5} C_{O_2} \exp\left(\frac{-12200}{T_g}\right) \quad (\text{Eq. 3-13})$$

3-3-4. Combustion of fixed carbon within the bed

Fixed carbon in a solid waste particle is combusted and described per the following equations:



$$\frac{CO}{CO_2} = 2500 \cdot \exp\left(\frac{-6420}{T}\right) \quad (\text{Eq. 3-15})$$

$$R_{C(\text{solid})} = \frac{C_{O_2}}{\left(\frac{1}{k_r} + \frac{1}{k_d}\right)} \quad (\text{Eq. 3-16})$$

Eq. (3-15) is char consumption rate expressed by Smoot and Pratt (Smoot and Pratt 1979)

Chapter 4: Discrete Element Method (DEM) numerical simulation of flow dynamics and mixing

4.1 Numerical Simulation

The discrete element method is a method that characterizes particle systems by modeling each particle and its interactions with its surroundings individually and over time. In this manner, the motion of a particle is computed by calculating all forces acting on it while integrating the equations of motion numerically. The dynamics of each particle are determined by the forces and torques acting on a particle. The translational motion of a particle is described by the equation of Newton's 2nd law. It is expressed by the inertia and the forces acting at the centre of gravity of a particle i . This governing equation can be written as:

$$m_i \frac{d^i v_i}{dt} = m_i a_i = \sum F_{i,Contact} + g \quad (\text{Eq. 4-1})$$

$$v_i = \frac{dx_i}{dt}$$

Above, m_i , v_i , a_i , F_i and x_i represent the particle mass, the particle velocity, the particle acceleration, the particle contact force and the position vector, respectively, g denotes the vector of gravity acceleration.

$$F_{i,Contact} = \sum_{j=1, j \neq i}^N F_{ij}$$

$F_{i,Contact}$ is composed by forces acting at the center of mass of the particles when there is contact between a particle and its surroundings.

The force \vec{F}_i of a particle is composed of the following parts:

$$\vec{F}_i = \vec{F}_{i,Contact} + \vec{F}_{i,Buoyancy} + \vec{F}_{i,Fluid} \text{ where } \vec{F}_{i,Fluid} \text{ are the fluid drag forces.}$$

$\vec{F}_{i,Buoyancy}$ comprises the buoyancy force of a particle in a surrounding fluid due to differences between the densities of a particle and the surrounding fluid and can be written as follows:

$$\vec{F}_{i,Buoyancy} = V_i (\rho_i - \rho_{Fluid}) \cdot \vec{g}$$

where V_i , ρ_i , ρ_{Fluid} and \vec{g} are the volume of a particle, the density of a particle, the density of the fluid, and the gravity acceleration vector, respectively. If the

fluid density is negligible, the buoyancy force equals the gravity force and the fluid drag force $\vec{F}_{i,Fluid}$ equal to zero.

Newton's and Euler's equations

$$m_i \frac{d^2 \vec{x}_i}{dt^2} = \sum_{j=1}^N \vec{F}_{ij} + m_i \vec{g} \quad (\text{Eq. 4-2})$$

$$J_i \frac{d^2 \vec{\varphi}_i}{dt^2} = \sum_{j=1}^N \vec{M}_{ij} \quad (\text{Eq. 4-3})$$

Above m , J , $d^2 \vec{x}_i / dt^2$, $d^2 \vec{\varphi}_i / dt^2$, \vec{M} denote respectively the particle mass, moment of inertia, acceleration, angular acceleration, the translational and rotational motion external moments; it is expressed by the inertia and the forces acting at the centre of gravity of a particle i . The contact forces can be decomposed in their normal and tangential components for the force balance within the equations of motion. External moments that affect rotational motion are caused by tangential forces, and gravitational forces must be considered. After all forces involved are determined, the equations of motion are numerically integrated (Allen et al. 1987).

In a discrete element model particles are assumed to be rigid. However, in order to model their deformation during collision they are permitted to overlap each other (Johnson, 1989), provided that the overlap, e.g. deformation, is much smaller than the particle size. According to Kruggel-Emden et al. 2007, this overlap is defined by:

$$\delta = \frac{1}{2}(d_i + d_j) - (x_i - x_j) \cdot n \quad (\text{Eq. 4-4})$$

where d_i, d_j are the particle diameters and x_i, x_j are the positions of the particle centers, with the normal vector n pointing from the center of particle j to i . The normal velocity of the contact point of particle i while overlapping particle j can be derived from the particle velocities v_i and v_j as

$$v_n = -\left((v_i - v_j) \cdot n \right) \cdot n \quad (\text{Eq. 4-5})$$

The vector n is defined as $n = (x_i - x_j) / |x_i - x_j|$

By an approach based on the overlap and the normal velocity it is possible to model the normal force during contact of two particles or a particle and a wall as

$$\mathbf{F}^n = F_{el}^n + F_{diss}^n = k^n \delta n + \gamma^{nv} \mathbf{r}_n \quad (\text{Eq. 4-6})$$

where k^n is the elastic constant of the material and γ^n is the normal energy dissipation coefficient. This force model can be applied in this study leading to a constant coefficient of normal restitution and a constant collision time that is independent of the initial normal velocity v_0 .

Equation number (3-7) models the relative velocity of a particle

$$v_{ij} = (v_i - v_j) - \frac{1}{2}(\omega_i d_i + \omega_j d_j) \cdot \mathbf{n} \quad (\text{Eq. 4-7})$$

and the tangential velocity of a particle contact point is given by

$$v^t = v_{ij} - (v_{ij} \cdot \mathbf{n}) \cdot \mathbf{n} \quad (\text{Eq. 4-8})$$

The angular velocities of the particles in a collision are denoted by ω_i and ω_j .

The tangential force F^t will be given, according to Newtonian mechanics, and the following equation model that was first introduced by Cundall and Strack (1979).

$$F^t = \min\{\mu_c F, k^t \int v^t dt + C^t v^t\} \quad (\text{Eq. 4-9})$$

where k^t is the stiffness of a linear spring and μ_c is the Coulomb friction coefficient. At the time of a contact of two particles a spring is designated between both of them and it is stretched or shortened while the particles stay in contact, it can be interpreted as a linear spring limited by the Coulomb friction.

Equation (4-10) denotes the tangential stiffness k^t derived by Kruggel-Emden et al. 2007, from an elastic case studied by Maw et al. 1976.

$$k^t = km \frac{\pi^2}{(t^n)^2} \quad (\text{Eq. 4-10})$$

k represents the tangential-to-normal stiffness ratio and t^n represents how long this contact lasts. The stiffness ratio can be determined from the mechanical properties of the particles included in the collision, as specified below:

$$k = \frac{[(1 - \nu_i)/G_i] + [(1 - \nu_j)/G_j]}{[(1 - 0.5\nu_i)/G_i] + [(1 - 0.5\nu_j)/G_j]} \quad (\text{Eq. 4-11})$$

where ν represents the Poisson ratio and G the shear modulus of two collided particles i and j .

Discrete Element Simulations (DEM) use mostly linear models. To be able to include energy dissipation their normal force F^n has two parts, one for modeling the elastic repulsion (elastic spring), the other for the viscous dissipation (displacement rate dependent damper), as denoted on Equation (4-6). This equation has an analytic solution derived by Schafer et al. 1996, and leads to a constant coefficient of restitution and a constant duration of collision independent of v_0 given by:

$$e^n = \exp\left(-\frac{\gamma^n}{2m} \pi \left(\frac{k^n}{m} - \left(\frac{\gamma^n}{2m}\right)^2\right)^{-1/2}\right), \quad (\text{Eq.4-12})$$

$$t^n = \pi \left[\frac{k^n}{m} - \left(\frac{\gamma^n}{2m}\right)^2\right]^{-1/2} \quad (\text{Eq.4-13})$$

A review and evaluation of normal forces can be found in (Kruggel-Emden et al. 2007) for normal forces and for tangential forces.

The simulation of mechanical motion of waste is difficult due to the different types of geometries involved. They could be approximated with clustered, as spherical or elliptic, but it would increase computing time significantly, especially when we consider heat, mass transfer and chemical reactions. Taking this into consideration, the simulations are using "representative" spheres only and the information regarding contact is derived from the spherical geometry.

4-1-1. Dynamics of mixing

The following equations describe the intensity of mixing for particles on a roller and reverse acting grates. They are based on two different approaches for understanding the dynamics of mixing first introduced by Peters et al. 2005 on their work on forward acting grate.

4-1-2. Proposal based on particles' velocity

The particles' velocity v_i at a time t can be specified in a average velocity \bar{v} and fluctuating component v' as

$$v_i(t) = \bar{v}_i(t) + v'_i(t) \quad (\text{Eq. 4-14})$$

the average velocity \bar{v} is obtained by averaging the all particles' velocity that fulfill the condition δ_{ij}^V defined on equation (4-15)

$$\bar{v}_i(t) = \frac{\sum_{j=1}^n \delta_{ij}^V v_j}{\sum_{j=1}^N \delta_{ij}^V} \quad (\text{Eq. 4-15})$$

The condition δ_{ij}^V it is defined as a logical binary one and it is satisfied for all particles j , which are closer to a particle i than the radius of the particle surrounding volume and is defined as r_V :

$$\delta_{ij}^V = 1 \text{ if } |x_j - x_i| \leq r_V, \quad \delta_{ij}^V = 0 \text{ if } |x_j - x_i| > r_V \quad (\text{Eq. 4-16})$$

The fluctuating velocities of the particles at a specific time can be used to give the local horizontal and vertical averaged mixing on the grate. The time dependent mixing parameters in x and y directions $p_x(x,t)$ and $p_y(x,t)$, also the total mixing parameter $p(x,t)$ are denoted below:

$$p_x(x,t) = \frac{\sqrt{\sum_{i=1}^N v_{x,i}^2 \delta_i^{\Delta x}}}{\sqrt{\sum_{i=1}^N \delta_i^{\Delta x}}} \quad (\text{Eq. 4-17})$$

$$p_y(x,t) = \frac{\sqrt{\sum_{i=1}^N v_{y,i}^2 \delta_i^{\Delta x}}}{\sqrt{\sum_{i=1}^N \delta_i^{\Delta x}}} \quad (\text{Eq. 4-18})$$

Similarly it is possible to define, based on the absolute value of the fluctuating velocity, a scalar mixing property $p(x,t)$ as

$$p(x,t) = \frac{\sqrt{\sum_{i=1}^N |v'_i| \delta_i^{\Delta x}}}{\sqrt{\sum_{i=1}^N \delta_i^{\Delta x}}} \quad (\text{Eq. 4-19})$$

A binary condition $\delta_i^{\Delta x}$ is used in the equation above to allow properties p_j and p relating on a local position along the grate. This condition averages equations (4-18) and (4-19) are resulting on particles being placed next to $x(\Delta x)$:

$$\delta_i^{\Delta x} = 1, \text{ if } |x_i(t) - x| \leq \Delta x / 2, \delta_i^{\Delta x} = 0 \text{ if } |x_i(t) - x| > \Delta x / 2 \quad (\text{Eq. 4-20})$$

According to Kruggel-Emden et al. 2007 the mixing properties listed above are averaged over the simulation time in discrete element steps $[Nt_1, Nt_2]$, and resulting $P'_i(x)$ and $P'(x)$ as the time-averaged vectorial mixing and the scalar mixing properties, respectively.

$$P'_x(x) = \frac{\sqrt{\sum_{j=N_1}^{N_2} p_{x,j}^2(x,t)}}{\sqrt{(Nt_2 - Nt_1)}} \quad (\text{Eq. 4-21})$$

$$P'_y(x) = \frac{\sqrt{\sum_{j=N_1}^{N_2} p_{y,j}^2(x,t)}}{\sqrt{(Nt_2 - Nt_1)}} \quad (\text{Eq. 4-22})$$

$$P'(x) = \frac{\sqrt{\sum_{j=N_1}^{N_2} p_j^2(x,t)}}{\sqrt{(Nt_2 - Nt_1)}} \quad (\text{Eq. 4-23})$$

4-1-3. Proposal based on the particles' trajectory

This proposal is based on analyzing the change of particle position in a packed bed. The DEM modeling code used on this study traces the position of a particle during the complete simulation time. The quantity for vertical mixing is obtained, taking into account the particle change in vertical position over the height of the packed bed. Assuming that a particle i at time t is defined as $x_i(t)$ and $y_i(t)$ for horizontal and vertical directions, respectively. Subsequently, the height of the packed bed $h(x_i, t)$ above the grate at a position x and a time t above the grate at a position x_i and a time t is defined as

$$h(x_i, t) = y_{top}(x_i, t) - y_{bottom}(x_i, t) \quad (\text{Eq.4-24})$$

The formula shows the top and bottom positions of packed bed at a time t and a position $x_i(t)$ of a particle i . All particles at a certain time t need to be selected with the condition $\delta_i^{\Delta x}$ for their y coordinate as follows

$$y_{top}(x_i, t) = \max(y_j \delta_j^{\Delta x}) \text{ and } y_{bottom}(x_i, t) = \min(y_j \delta_j^{\Delta x}) \quad (\text{Eq. 4-25})$$

The expression written below specify a normalized particle depth, it when applied can give data on the average depths of particles of a specified size within a specified region along the grate length. A particle at the top of the structure has a normalized depth of $D_i = 0$ and at the bottom of $D_i = 1$.

$$D_i(t) = [y_{top}(x_i, t) - y_i(t)] / h(x_i, t) \quad (\text{Eq. 4-26})$$

The average depths of particles as described above can be represented by

$$D^L(d', d'', t) = \sum_{i=1}^N D_i(t) \delta_i^x \delta_i^d / \sum_{i=1}^N \delta_i^x \delta_i^d \quad (\text{Eq. 4-27})$$

The condition δ_i^x screens particles into a specified interval as

$$\delta_i^x = 1 \text{ if } (x_1 \leq x_i(t) \leq x_2), \delta_i^x = 0 \text{ if } (x_1 > x_i(t)) \vee (x_2 < x_i(t)) \quad (\text{Eq. 4-28})$$

The other condition δ_i^d screens particles into the following diameter range:

$$\delta_i^d = 1 \text{ if } (d' \leq d_i \leq d''), \delta_i^d = 0 \text{ if } (d' > d_i) \vee (d'' < d_i) \quad (\text{Eq. 4-29})$$

The particles depths variable to be useful in this study needs to provide data regarding the dynamics of mixing. Then, it needs to be averaged and also its fluctuating component needs to be derived as it was previously done for the particle's velocity on equation (3-14) leading to

$$D_i(t) = \bar{D}_i(t_1, t_2, x_1, x_2) + D'_i(t) \quad (\text{Eq.4-30})$$

The average value of an averaged depth is calculated over time and lengths as

$$\bar{D}_i(t_1, t_2, x_1, x_2) = \frac{\sum_{j=Nt_1}^{Nt_2} \sum_{i=1}^N D_{i,j}(t) \delta_i^x}{\sum_{j=Nt_1}^{Nt_2} \sum_{i=1}^N \delta_i^x} \quad (\text{Eq.4-31})$$

A vertical mixing property can be developed from the fluctuating particle depths in the form of a standard deviation averaged over time for a specific position x as,

$$M^t(x) = \frac{\sqrt{\sum_{j=Nt_1}^{Nt_2} \sum_{i=1}^N D'_{i,j}(t) \delta_i^{\Delta x}}}{\sqrt{\sum_{j=Nt_1}^{Nt_2} \sum_{i=1}^N \delta_i^{\Delta x}}} \quad (\text{Eq. 4-32})$$

4-2. Simulation parameters and geometric features of the roller grate

The rolls used in the design of the grate layout is modeled by line segments in a two dimensional DEM simulation. The geometry of the roller grate is based on a grate furnace operated at Essex County in New Jersey by Covanta, and sketched in Figure 1; its geometry is chosen to have the same grate length as the reverse acting grate modeled by Nakamura, 2007. As a continuation of this study, another model using simulation parameters from Nakamura's work will be applied using the DEM code. It will then be possible to compare outputs between the roller grate and the reverse acting grate based on a grate furnace operated at Union County in New Jersey by Covanta. We will also compare previous results from Nakamura's research, where he used the Markov chain model.

The roller grate on this study has a length of $L=7$ meters, it is equipped with six rolls of radius $r= 0.455$ meters. The void space between the rolls is $b= 0.227$ meters. The declination of the grate is chosen with $\alpha = 16$ deg. Only between the last rolls the declination is reduced to $\alpha = 8$ deg. The operational conditions are chosen according to Table 1, with the first roll rotating slightly faster than the remaining rolls.

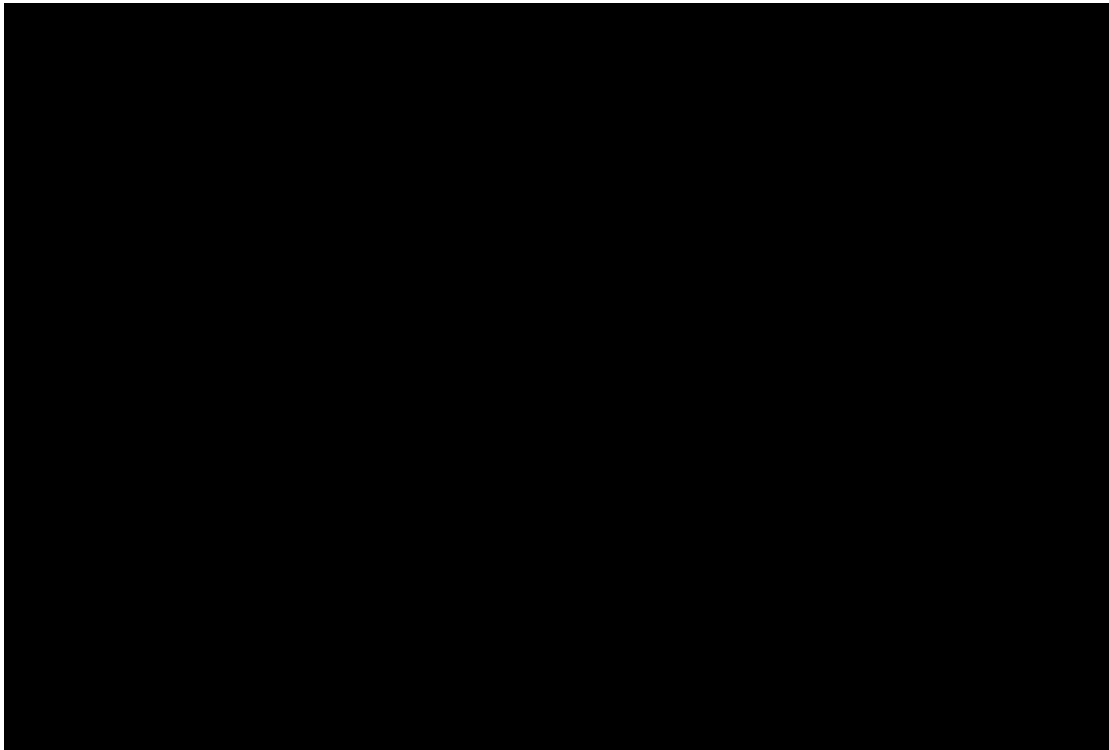


Figure 4-1. Two dimensional sketch of roller grate

For the simulations, the granular material is assumed to consist of spherical particles made out wood. The necessary mechanical properties are summarized in Table 4-2. The dynamic properties describing the interactions between particles and the interaction of particles with walls are chosen as constant. The dynamic interaction properties are realized with the force models specified in Sec. 4.1.

Rolls	1	2-6
Velocity (1/s)	0.025	0.02

Table 4-1: Kinectics of the Düsseldorf process. David H. F. Liu and Béla G. Lipták 1999.

Density ρ	700 Kg / m^3
Young's modulus E	10.0 MPa
Shear modulus G	3.0 Mpa
Normal coefficient of restitution e^n	0.3
Dynamic friction coefficient (particle/particle) $\mu_{C,PP}$	0.5
Dynamic friction coefficient (particle/wall) $\mu_{C,PW}$	0.5

Table 4-2: Particle data. Peters et al. 2004 and Kruggel-Emden et al. 2007.

The linear stiffness in normal direction is fixed with $k^n = 1000$ N/m. The normal damping constants $\gamma^n = 0.3$ are calculated to match the normal coefficient of restitution of $e^n = 0.3$ both for particle/particle and particle/wall contacts. The normal to tangential spring ratio k is calculated according to Di Maio et al. 2004. Using this ratio, the tangential stiffness was calculated using equation 3-10. The material parameters of the model for particle/particle and particle/wall interactions are specified in Table 3-3 and the particle's size distribution are specified in Table 3-4.

The mixing properties were calculated in an area from $x_1 = 0$ m to $x_2 = 7$ m.

	Particle/Particle	Particle/Wall
Normal spring constant [N/m] K^n	1000	1000
Normal damping constant [kg/s] γ^n	0.01-0.017	0.030-0.035
Normal-to-tangential spring ratio k	0.87	0.86
Tangential spring constant [N/m] k^t	870	860

Table 4-3: Material parameters of the model for particle/particle and particle/wall interaction.

Particles	Diameter (m)	Number in 2D roller grate
1	0.0083	198
2	0.0157	198
3	0.0227	198
4	0.0298	198
5	0.0367	198

Table 4-4: Particle size distribution.

4-2-1. Conclusions for the roller grate numerical simulation

The roller grate simulations were accomplished in two dimensions. The setup of the simulation of the roller grate is similar to the mathematical modeling study done by Peters et al. 2004 for the forward acting grate. The calculations were performed on a x86_64 Intel server running RedHat Enterprise Linux 5.0. It is assumed that particles with different sizes are randomly distributed. The initial bed height differentiates over the bed length. The largest particles are concentrated in the middle of the bed because of gravitational influences related to the angle declination.

Figure (4-2) shows the time-averaged horizontal, vertical, and total mixing parameters $P'_i(x)$ and $P'(x)$. We can observe that the most intense mixing takes place in void spaces close to the rolls of the grate. Particles are moved downward on the right side and upward on the left side of a roll according to the rotational motion of the rolls, in that way it induces vortices in the void spaces between the rolls. We also can notice that the most prominent mixing happens right before roll number 2, and being almost uniform for spaces between the other rolls.

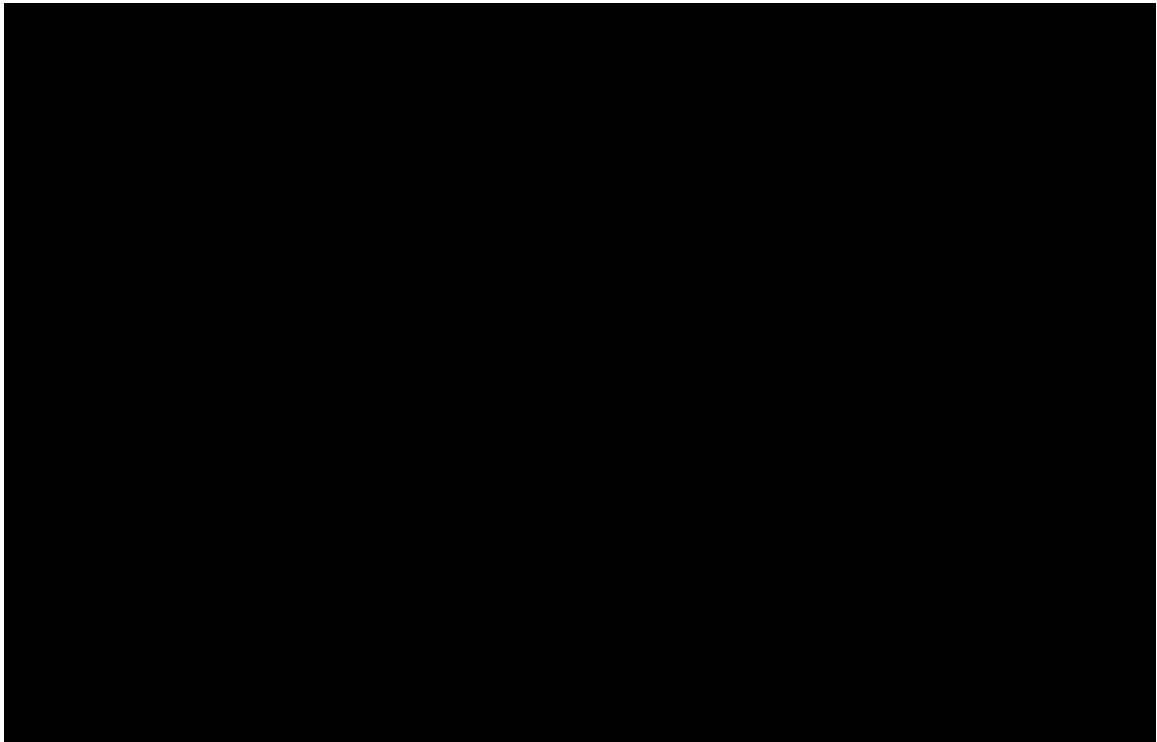


Figure 4-2. Time-averaged horizontal, vertical and total mixing parameters the grate length.

The time-averaged vertical mixing parameter $M^l(x)$ on Figure (4-3) is a property that quantifies the local mixing. The tendencies in Figures (4-2) and (4-3) are very similar. The mixing parameter $M^l(x)$ shows a very harmonic trend probably because of the very symmetric geometry of the roller grate. The intense mixing parameter near the end of the grate can be attributed as an effect of the exit zone.



Figure 4-3. Time-averaged mixing parameter over the grate length.

The average depth of different particles over time is showed in Figure (4-4). The motion of the roller grate affects segregation of particles. We can observe that after a time span of $t = 500$ s, the average depth gets to a steady state. The small particles are most likely to be localized at the top layer of the packed bed, while large particles are at the low depth.

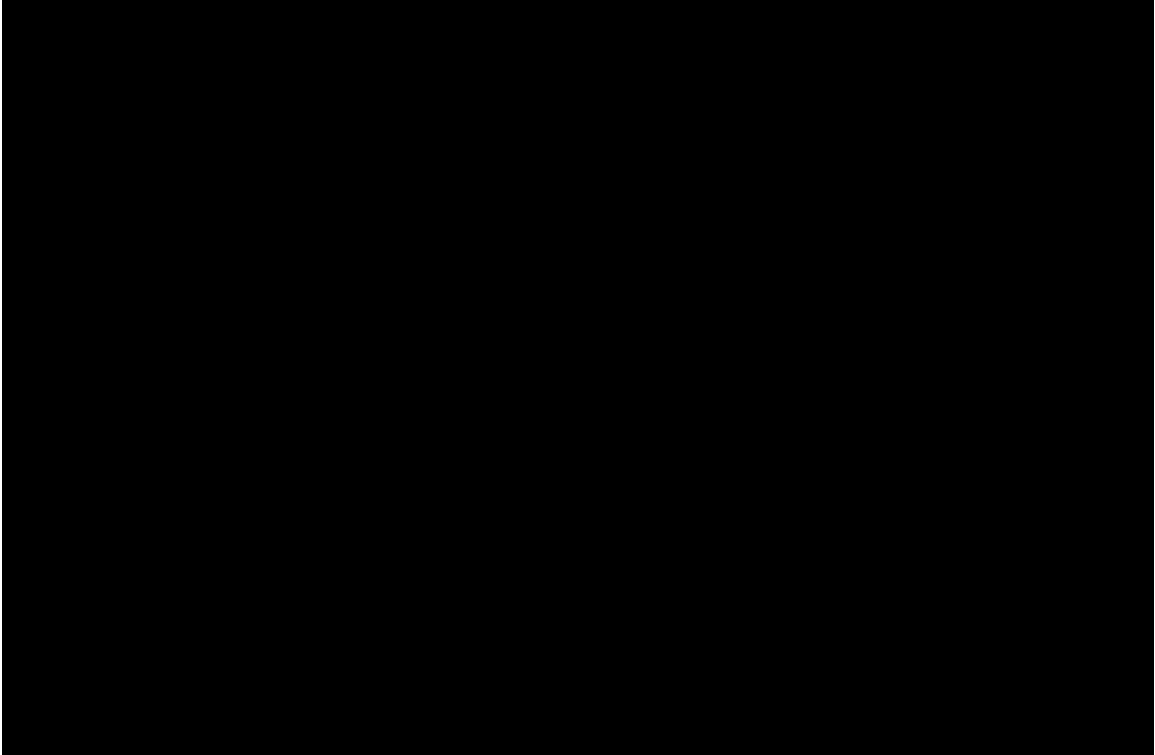


Figure4- 4. Average normalized depth for different particle diameters

4-3. Simulation parameters and geometric features of the reverse acting grate

The bars used in the design of the grate layout is modeled by line segments in a two dimensional DEM simulation. The geometry of the reverse acting grate is based on a grate furnace operated at Union County in New Jersey by Covanta, and sketched in Figure 5; its geometry is chosen to have the same grate length as the reverse acting grate modeled by Nakamura, 2008.

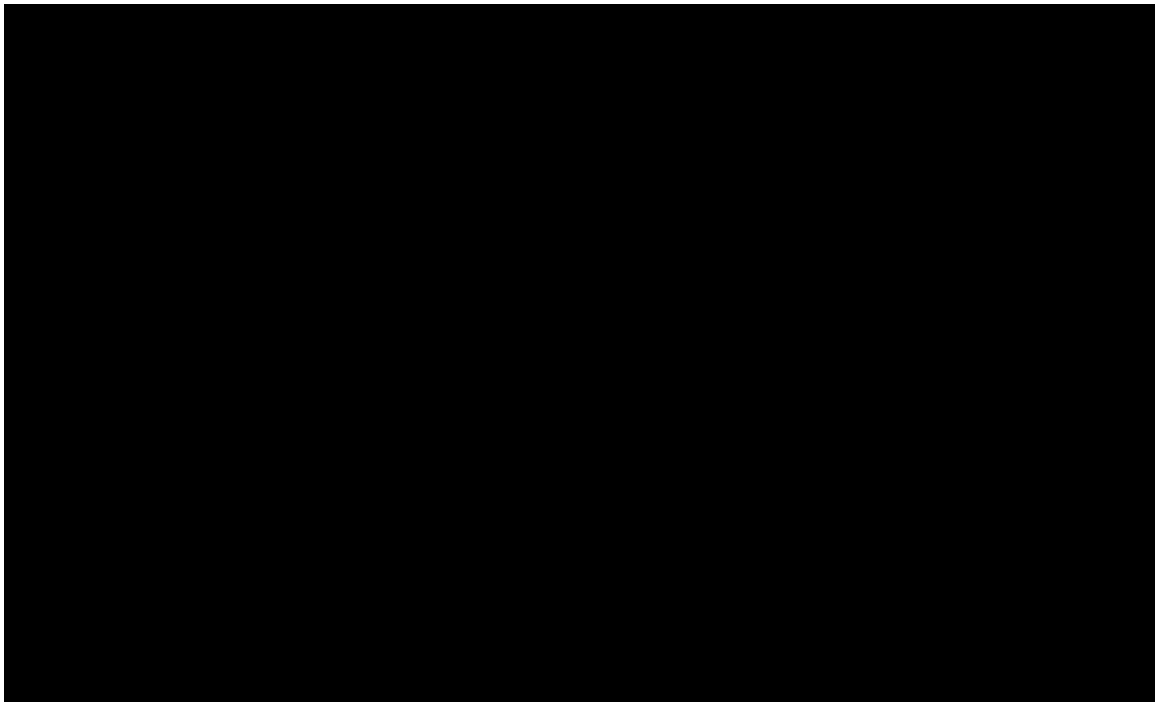


Figure 4-5. Two dimensional sketch of reverse acting grate.

The reverse acting grate on this study has a length of $L=7$ meters, it is equipped with 15 bars and is inclined about 26 degrees to the horizontal. The bars are positioned at an angle of 13 degrees from the traveling bed. Eight of the 15 bars are reciprocating and move a distance of 0.42 m (420 mm). The frequency of motion of the reciprocating bars can be adjusted from 10 to 50 double strokes per hour. A typical operating frequency in a WTE unit is 12 strokes per hour but the frequency used depends greatly on the composition of the MSW feed.

A typical feed rate of MSW into the combustion chamber is 18.1 metric tons per hour (WTE of 480 short tons per day capacity). The average density of MSW is 500 lb per yd³ or 173.2 kg per m³ (Tchobanoglous *et al.* 1993) .Therefore, the corresponding volumetric feed rate of MSW is 104.8 m³ per hour. A typical ratio of the downward volumetric flow rate of MSW feed to the upwards flow of waste due to the motion of the reciprocating bars (volume of material pushed upward by the bar motion) is approximately 5/1.

For the simulations, the granular material is assumed to consist out of spherical particles made of wood. The necessary mechanical properties are summarized in Table 4-2. The operating conditions are chosen according to Nakamura's 2008 research work and are listed in Table 4-5. An example of the MSW flow and mixing agitated by reverse acting grate are showed in Table 4-6. The dynamic properties describing the interactions between particles and the interaction of particles with walls are chosen as constant. The dynamic interaction properties are realized with the force models specified in Sec. 4-1. The linear stiffness in normal direction, the normal damping constants, the normal to tangential spring ratio and the tangential stiffness were calculated using the same methods and values used for the roller grate as specified in Sec. 4-2. The material parameters of the model for particle/particle and particle/wall interactions are showed in Table 4-3, and the particle's size distribution are showed in Table 4-4.

Velocity (m/s)	0.011	0.011	0.010	0.010	0.010	0.005	0.005
Active bars	2	4	6	8	10	12	14

Table 4-5: Kinetics of the reverse acting grate.

The mixing properties area calculated in area from $x_1=0$ m to $x_2=7$ m. The particle bed height on the grates is chosen equal to guarantee the comparability between the different simulations in two dimensions. The radius being used in the average velocities calculations is $r_v = 0.08$ m.

Volume (m^3/s)	102.74	97.71	83.65	54.52	27.40	16.36	9.23
Active bars	2	4	6	8	10	12	14

Table 4-6: MSW flow and mixing in the reverse acting grate.

4-3-1. Conclusions for the reverse acting grate numerical simulation

The reverse acting grate simulations were accomplished in two dimensions. The setup of the simulation of the reverse acting grate is similar to the mathematical modeling study done by Peters et al. 2004 for the forward acting grate and also used data from Nakamura's research work 2008. The calculations were performed on a x86_64 Intel server running RedHat Enterprise Linux 5.0.

It is assumed that particles with different sizes are randomly distributed. The initial bed height diversifies over the bed length. The largest particles are concentrated in the middle of the bed because of gravitational influences related to the angle declination. The discrete element simulations were performed using an adapted ESys-Particle HPC code and MatlabR2009A for a better visualization of the graphics generated. The time span of the simulations covers the range $t = 150 - 4250$ s. The selected step size was $\Delta t = 2.3 \times 10^{-5}$ s.

Figure (4-5) shows the time-averaged horizontal, vertical, and total mixing parameters $P'_i(x)$ and $P'(x)$. Both parameters are based on the time-averaged deviation of the fluctuating and give an insight into the spatial localization of mixing processes. If a certain area on the grate is related to a more intense mixing, all mixing parameters are affected equally. This can be explained especially in a dense packing by the fact that a particle can only move if surrounding particles make way by moving in normal directions to the particle's trajectory. The most intense mixing happens at a position of $x=1.3$ m and $x=2.7$ m.

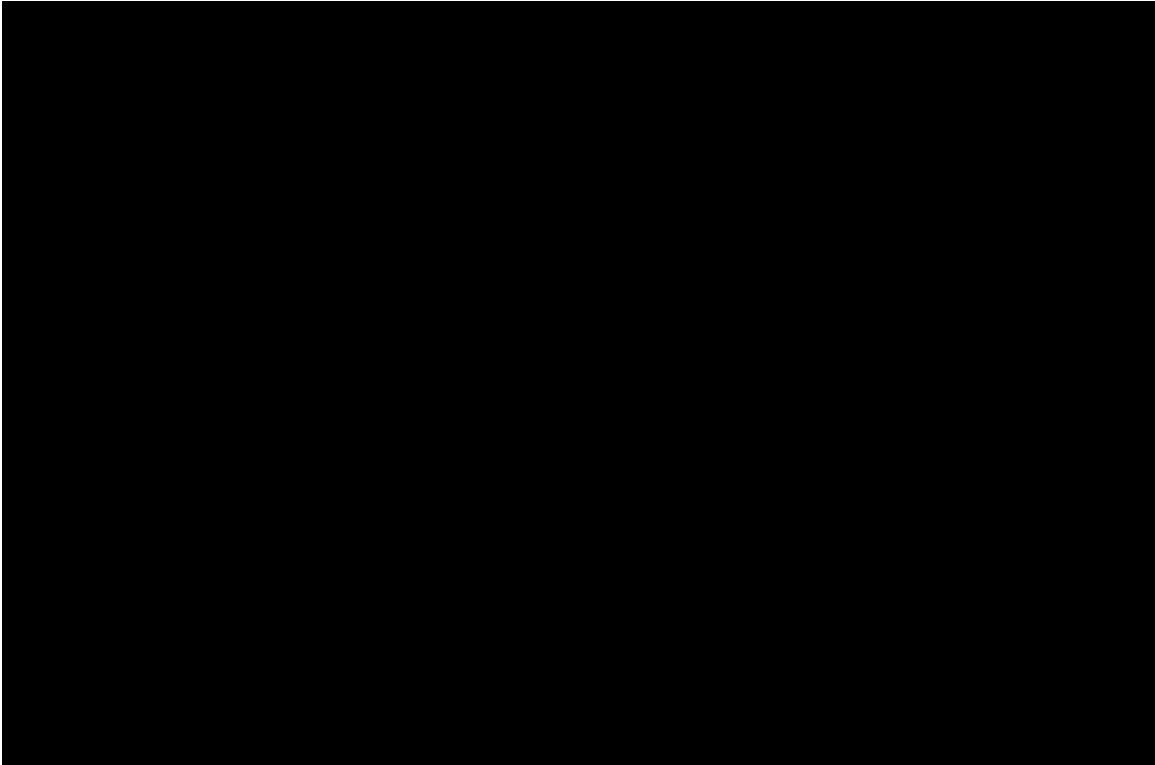


Figure 4-5. Time-averaged horizontal, vertical and total mixing parameters the grate length.

The time-averaged vertical mixing parameter $M^v(x)$ on Figure (6) is similar to $P_y^v(x)$ a property that quantifies the local mixing. The tendencies in Figures (5) and (6) are very similar if values for $x < 1$ m and $x > 6.3$ m are excluded. The behavior in these regions appears to be under the influence of the entry and exit of the grate. The mixing parameter $M^t(x)$ shows the lowest mixing in regions around $x = 5$ m.



Figure 4-6. Time-averaged mixing parameter over the grate length.

The average depth of different particles over time is showed in Figure (4-7), this parameter gives a insight into dynamics of segregation. The motion of the reverse acting grate affects segregation of particles, there is a tendency for particles to reorganize themselves in different layers. We can observe that after a time span of $t = 550$ s, the average depth gets to a steady state. The small particles are most likely to be localized at the top layer of the packed bed, while large particles are at the low depth and the average over all particles is lying in between.

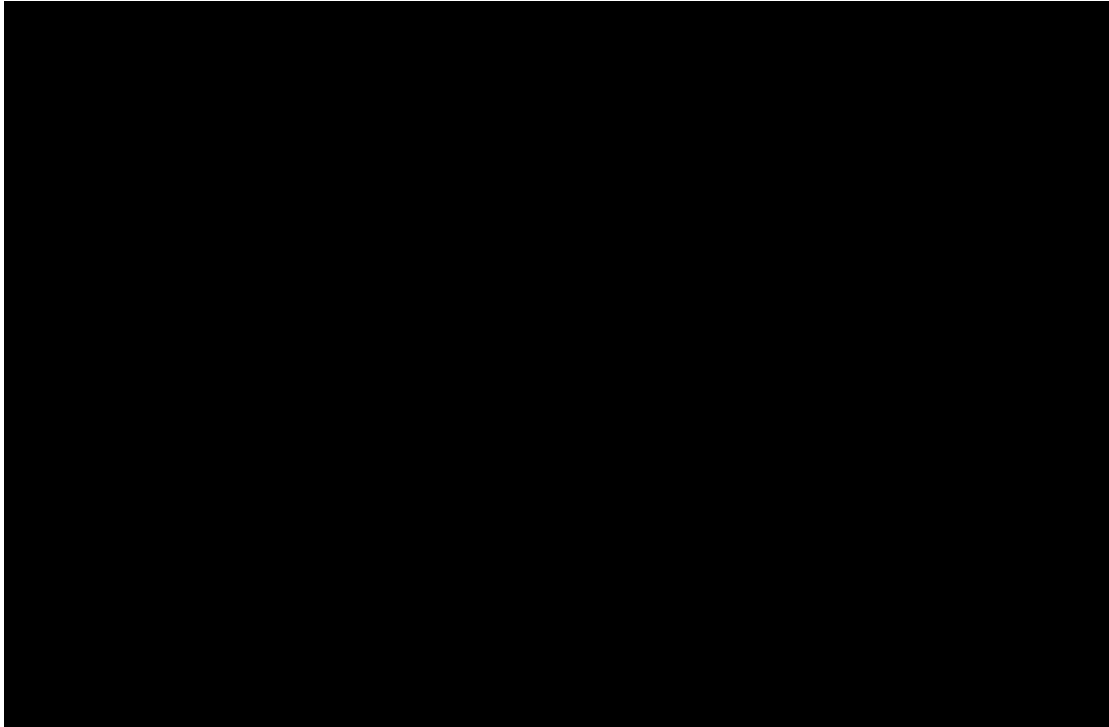


Figure 4-7. Average normalized depth for different particle diameters.

4-4. Conclusions and Suggested Further Research

On the basis of the model results, it was concluded that mixing on a roller grate is much more localized than mixing on a reverse acting grate. The time-averaged velocity dependent properties $P_i^t(x)$ were averaged over the grate length to obtain the overall mixing. This total mixing property was shown to be more intense for the roller grate than for the reverse acting grate. The more distributed mixing on the reverse acting grate is also apparent when

comparing the fluctuation of the normalized depth based property $M'(x)$. The dynamics of segregation on both grate designs show the same pattern.

Further research is necessary to collect information related to transportation of the waste material in the cross flow to a gaseous fluid modeling the furnace. An established commercial CFD/FLUENT code is suggested for use. To get a closer simulation of the combustion plant, the furnace model should be coupled to a model of the waste combustion on the three most prominent types of moving grate: The forward reciprocating grate of Von Roll, the Martin reverse-acting grate, and the Roller grate (Dusseldorf System).

BIBLIOGRAPHY

B. Peters, Measurements and application of a Discrete Particle Model (DPM) to simulate combustion of a packed bed of individual fuel particles, *Combustion and Flame* 131 (2002) 132–146.

B. Peters, A. Dziugys, H. Hunsinger, L. Krebs, An approach to quantify the intensity of mixing on a forward acting grate, *Chemical Engineering Science* 60 (2005) 1649–1659.

E. Rougier, A. Munjiza, N.W.M. John, Numerical comparison of some explicit time integration schemes used in DEM, *International Journal for Numerical Methods in Engineering* 61 (2004) 856–879.

H. Kruggel-Emden, Analysis and Improvement of the Time-driven Discrete Element Method, Doctor Thesis, Bochum, 2007b.

H. Kruggel-Emden, E. Simsek, S. Rickelt, S. Wirtz, V. Scherer, Review and extension of normal force models for the discrete element method, *Powder Technology* 171(3) (2007) 157–173.

H. Kruggel-Emden, E. Simsek, S. Wirtz, V. Viktor, A comparative numerical study of particle mixing on different grate designs through the discrete element method, *Journal of Pressure Vessel Technology* 129 (4) (2007).

H. Kruggel-Emden, E. Simsek, S. Wirtz, V. Scherer, A Comparison and Validation of Tangential Force Models for the Use within Discrete Element Simulations, DEM07 Conference, 2007, pp. 27–29, August 2007, Brisbane.

Hornbeck RW. *Numerical Methods*. Quantum Publishers, 1975.

Kumar Sudhir, "Technology options for municipal solid waste-to-energy project." *TERI Information Monitor on Environmental Science*, volume 5, June 2000.

Kunii, Daizo and Octave Levenspiel. *Fluidization Engineering*. 2nd ed. Boston: Butterworth-Heubemann, 1991.

Li, J. H. & Kwaauk, M (2003). Exploring complex systems in chemical engineering – the multi-scale methodology. *Chem. Eng. Sci.*, 58, 521-535.

M.A. Field, D.W. Gill, B.B. Morgan, P.G.W. Hawskley, *Combustion of pulverized coal*. The British Coal Utilization Research Association, 1967

Nakamura, M., H. Zhang, K. Millrath, and N.J.Themelis (2003):"Modeling of Waste-to-Energy Combustion with Continuous Variation of the Solid Waste Fuel." Proceedings of ASME IMECE, Washington, D.C.

Perry, Robert H. and Don W. Green. Perry's Chemical Engineers' Handbook. 7th Ed. New York: McGraw-Hill, 1997.

Reh, L. (1999). Challenges of circulating fluid-bed reactors in energy and raw materials industries. Chem. Eng. Sci., 54(22), 5359-5368.

P.A. Cundall, O.D.L. Strack, Discrete numerical model for granular assemblies, G´eotechnique 29 (1) (1979) 47–65.

S. Rickelt, S. Wirtz, V. Scherer, A new approach to simulate transient heat transfer within the discrete element method, Pressure Vessels and Piping Division Conference, Chicago, 2008.

S.Wirtz, F. Krüll,Modelling of waste grate firing for a complete furnace simulation, IT3 Conference on Incinerator & Thermal Treatment Technologies, Salt Lake City, 1998.

Themelis, N.J. "An Overview of the global waste-to-energy industry," WTER, July-August 2003.

Themelis, N.J., Y.H.Kim, and M. Brady (2002): "Energy Recovery from New York City Solid Wastes". Waste Management and Research 20, pp. 223-233.

T.h. Klasen, K. Görner, Numerical calculation and optimization of a large municipal waste incinerator plant, Incinerator and flue gas treatment technologies, U.K., 1999

Turns, S. R.: An Introduction to Combustion. 2nd ed. The Pennsylvania State University, 2000.

"Using Chaos to improve Fluidized Bed Combustion." December 31, 1996.

Wakao N, Kaguei S. Heat and mass transfer in packed beds. NY, USA: Gordon & Breach; 1982.

W.L. Vargas, J.J. McCarthy, Conductivity of granular media with stagnant interstitial fluids via thermal particle dynamics simulation, International Journal of Heat and Mass Transfer 45 (2002) 4847–4856.